THE EFFECT OF AN AIR GAP ON THE COUPLING BETWEEN TWO PLANAR MICROSTRIP LINES

Technical Report

Prepared by

Atef Z. Elsherbeni, Vicente Rodriguez-Pereyra and Charles E. Smith

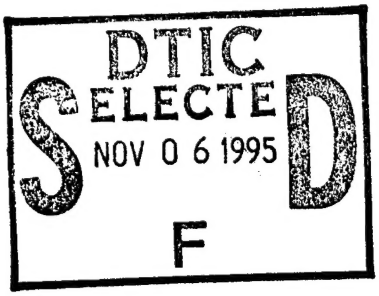

September, 1995

U. S. Army Research Office
Research agreement No.
DAAH04-94-G-0355

Technical Report No. 95-2
Department of Electrical Engineering
University of Mississippi

MASTER COPY KEEP THIS COPY FOR REPRODUCTION PURPOSES

REPORT DOCUMENTATION PAGE

Form Approved
OMB No. 0704-0188

1. AGENCY USE ONLY (Leave blank)

2. REPORT DATE: September 29, 1995

3. REPORT TYPE AND DATES COVERED: Technical Report

4. TITLE AND SUBTITLE

The Effect of an Air Gap on the Coupling Between Two Planar Microstrip Lines

5. FUNDING NUMBERS

DAAH04-94-G-0355

6. AUTHOR(S)

Atef Z. Elsherbeni, Vicente Rodriguez-Pereyra, and Charles E. Smith

7. PERFORMING ORGANIZATION NAME(S) AND ADDRESS(ES)

Department of Electrical Engineering
University of Mississippi
University, MS 38677

8. PERFORMING ORGANIZATION REPORT NUMBER

95-2

9. SPONSORING/MONITORING AGENCY NAME(S) AND ADDRESS(ES)

US Army Research Office
P.O. Box 12211
Research Triangle Park, NC 27709-2211

10. SPONSORING/MONITORING AGENCY REPORT NUMBER

11. SUPPLEMENTARY NOTES

The views, opinions and/or findings contained in this report are those of the author(s) and should not be construed as an official Department of the Army position, policy, or decision, unless so designated by other documentation.

12a. DISTRIBUTION/AVAILABILITY STATEMENT

Approved for public release; distribution unlimited.

12b. DISTRIBUTION CODE

13. ABSTRACT (Maximum 200 words)

The finite difference (FD) technique is used to investigate the air gap effect on the coupling between two planar microstrip lines. The strip lines are embedded between a dielectric substrate and a dielectric overlay. The air gap between the substrate and the overlay is present due to the thickness of the strips and/or the roughness of the planar surfaces. A quasi-static FD technique based on the solution of Laplace's equation is used to solve for the potential distribution in the region around the strips. The FD mesh is truncated by an artificial boundary to allow for a numerical solution with the available computer resources. At this artificial boundary an approximate boundary condition is used to truncate the FD mesh. From the potential distribution, the charge and the capacitance and inductance matrices of the stripline system are evaluated. The coupling or cross-talk between the lines are then defined and computed. The effects of the conducting strips thickness and the properties of the materials between the strips on the coupling are illustrated through numerical examples.

14. SUBJECT TERMS

Crosstalk, Transmission line coupling.

15. NUMBER OF PAGES

16. PRICE CODE

17. SECURITY CLASSIFICATION OF REPORT	18. SECURITY CLASSIFICATION OF THIS PAGE	19. SECURITY CLASSIFICATION OF ABSTRACT	20. LIMITATION OF ABSTRACT
UNCLASSIFIED	UNCLASSIFIED	UNCLASSIFIED	UL

ABSTRACT

The finite difference (FD) technique is used to investigate the air gap effect on the coupling between two planar microstrip lines. The strip lines are embedded between a dielectric substrate and a dielectric overlay. The air gap between the substrate and the overlay is present due to the thickness of the strips and/or the roughness of the planar surfaces. A quasi-static FD technique based on the solution of Laplace's equation is used to solve for the potential distribution in the region around the strips. The FD mesh is truncated by an artificial boundary to allow for a numerical solution with the available computer resources. At this artificial boundary an approximate boundary condition is used to truncate the FD mesh. From the potential distribution, the charge and the capacitance and inductance matrices of the stripline system are evaluated. The coupling or cross-talk between the lines are then defined and computed. The effects of the conducting strips thickness and the properties of the materials between the strips on the coupling are illustrated through numerical examples.

ACKNOWLEDGEMENT

This work was supported by the Army Research Office under grant number DAAH04-94-G-0355.

TABLE OF CONTENTS

LIST OF FIGURES

Figure Page

LIST OF TABLES

LIST OF SYMBOLS

c	Speed of light (2.998×10^8)	(m/s)
C_{ii}	Self capacitance	(pF/m)
C_{ij}	Mutual capacitance	(pF/m)
$\bar{D}$	Displacement vector	(C/m^2)
$\bar{E}$	Electric field	(V/m)
h	Length	(m)
K	Electric inductance	(F/m)
k_{e12}	Coupling coefficient of the transmission line, from conductor 1 to 2	(dB)
k_{e21}	Coupling coefficient of the transmission line, from conductor 2 to 1	(dB)
L	Inductance	(H/m)
g	Length of the transmission line in the z-direction	(m)
ℓ	Contour surrounding a conductor	(m)
$\bar{n}$	Normal vector direction	(Dimensionless)
Q^i	Total charge on the *ith* conductor	(pC/m)
s	Surface	(m^2)
V_i	Scalar potential at grid point i	(V)
v_{oe}	Normalized even-mode phase velocity of the transmission line	(Dimentionless)
v_{oo}	Normalized odd-mode phase velocity of the transmission line	(Dimentionless)
x,y,z	Length in Rectangular coordinates system	(m)
Z_o	Characteristic impedance of the transmission line	(Ω/m)
Z_{oe}	Even-mode characteristic impedance of the transmission line	(Ω/m)
Z_{oo}	Odd-mode characteristic impedance of the transmission line	(Ω/m)
ϵ_{re}	Relative even-mode effective permittivity	(Dimentionless)
ϵ_{ro}	Relative odd-mode effective permittivity	(Dimentionless)
ρ,ϕ,z	Cylindrical coordinates system	(m,Radians,m)

CHAPTER I
INTRODUCTION

Over the past few decades, microstrip transmission lines have been analyzed extensively. Reducing the coupling has become very important, since as the clock rates in computers increase so does the effect of coupling or cross talk between the lines. The main purpose of this work is to analyze the effect of the air gap on the coupling between two planar microstrip lines. Two different geometries are analyzed using the finite difference (FD) technique. Figures 1 and 2 show the geometries where the striplines are perfectly embedded between the substrate and the overlay in contrast with Figs. 3 and 4 where an air gap is present due to the thickness of the strips and/or the roughness of the planar surfaces. Following the approach presented in [1], a FD technique based on the solution of Laplace's equation is used to find the potential distribution around the strips. From the potential distribution the charges on the strips are computed using Gauss' law and then the capacitance and inductances matrices are evaluated. The capacitive coupling between the lines is then computed. Numerical data are obtained for these strip line geometries with and without air gap in order to show the effects of the air gap on the coupling between the lines. The developed program is capable of solving different geometries of multi conductor transmission lines arbitrarily positioned in an inhomogeneous dielectric space. A FD mesh generator program is also developed to act as a preprocessor for the FD routine. Lagrangian polynomials are used to approximate the second order differential equation in Laplace's equation.Then, the integral form of Gauss's law is used to derive a general expression for the scalar potential at every point on the FD mesh. An Artificial Boundary Condition (ABC) is used to truncate the finite difference mesh to allow for a numerical solution with the available computer resources. The resulting expressions for the potential at the FD mesh points are cast into a matrix equation. Special arrangement of the points allow the use of a banded matrix solver for the solution of the related system of equations. From this solution of the matrix equation (i.e. the potential distribution), the electric field vectors are computed.

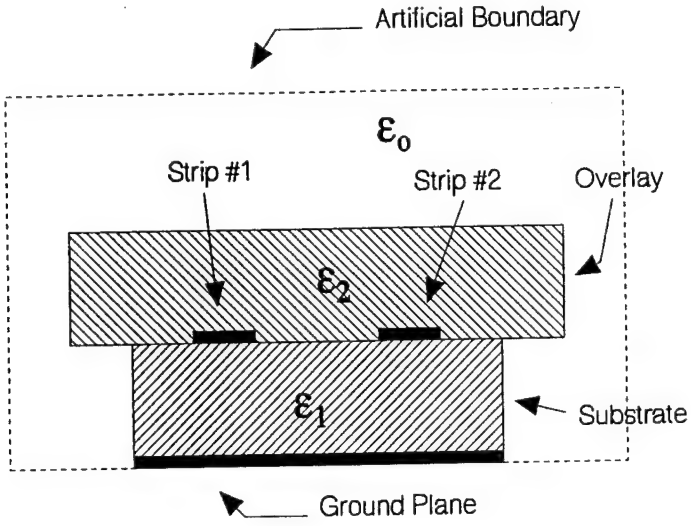

Fig. 1. A transmision line with two strips between the substrate and extended overlay (no air gap).

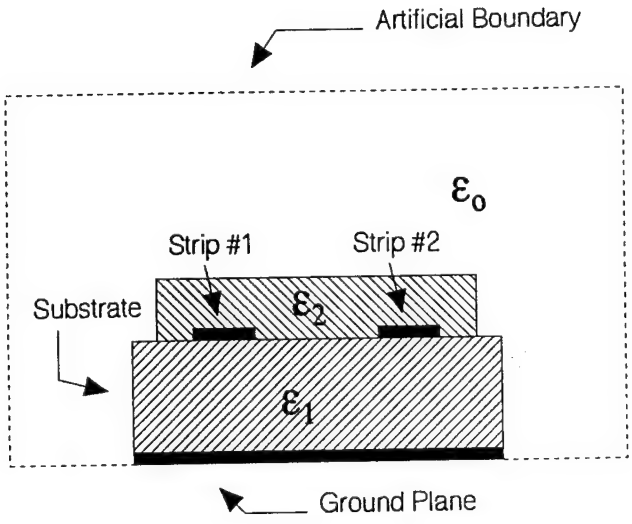

Fig. 2. A transmision line with two strips between the substrate and the dielectric overlay (no air gap).

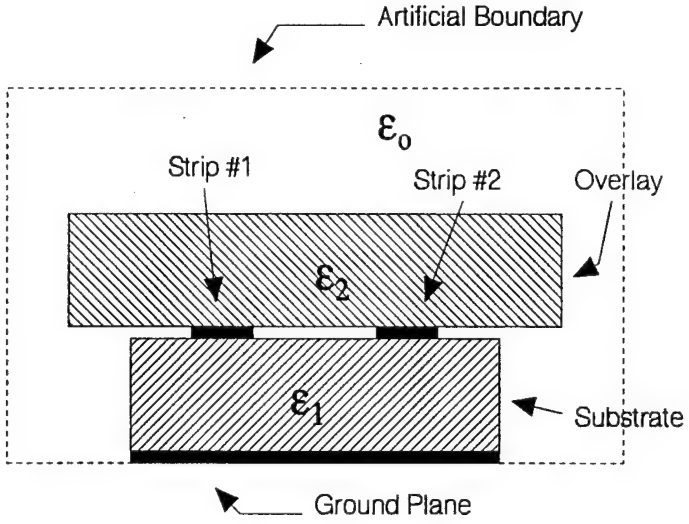

Fig. 3. A transmision line with two strips between the substrate and extended overlay (with air gap).

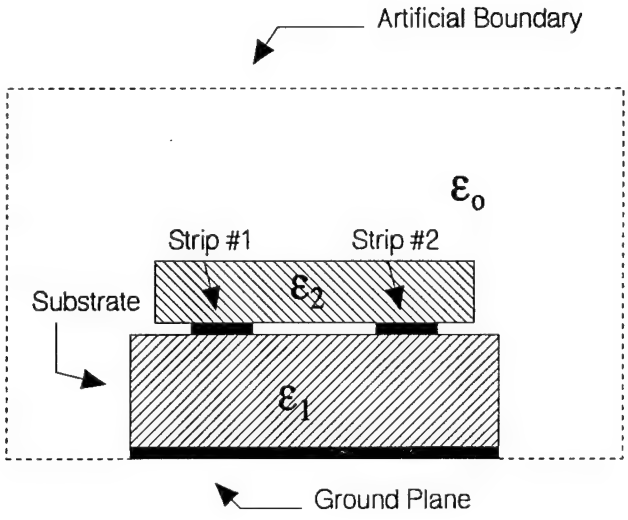

Fig. 4. A transmision line with two strips between the substrate and the dielectric overlay (with air gap).

CHAPTER II

FINITE DIFFERENCE FORMULATION

A) Finite Difference Approximation

Through the years, many methods have been developed for the analysis of microstrip transmission lines. Among those is the widely known finite difference technique. For the quasi-static 2D problems as shown in Figs. 1 to 4, the potential V can be described using Laplace's equation by:

$$\frac{\partial^2 V}{\partial x^2} + \frac{\partial^2 V}{\partial y^2} = 0 \tag{1}$$

The finite difference technique approximates the derivatives involved in Laplace's equation. This numerical approximation is based upon calculating the potential at a certain node as a function of neighboring grid points, or nodes.

In general, assuming three consecutive nodes L,C,R, as shown in Fig. 5, Lagrange's form of interpolating polynomial is described as [2]

$$f(x) \approx P_2(x) = \frac{(x-x_C)(x-x_R)}{(x_L-x_C)(x_L-x_R)} f(x_L) + \frac{(x-x_L)(x-x_R)}{(x_C-x_L)(x_C-x_R)} f(x_C) + \frac{(x-x_L)(x-x_C)}{(x_R-x_L)(x_R-x_C)} f(x_R) \tag{2}$$

where $P_2(x)$ represent a second degree polynomial which coincides with the exact values of the function $f(x)$ at the three nodes L,C,R. In order to apply Laplace's equation over the potential $V(x,y)$, the second order derivatives need to be approximated in both the x and y directions. The Lagrange interpolating polynomial will then have to be differentiated twice, that is

$$\frac{df(x)}{dx} = \frac{(x-x_C)+(x-x_R)}{(x_L-x_C)(x_L-x_R)} f(x_L) + \frac{(x-x_L)+(x-x_R)}{(x_C-x_L)(x_C-x_R)} f(x_C) + \frac{(x-x_L)+(x-x_C)}{(x_R-x_L)(x_R-x_C)} f(x_R) \tag{3}$$

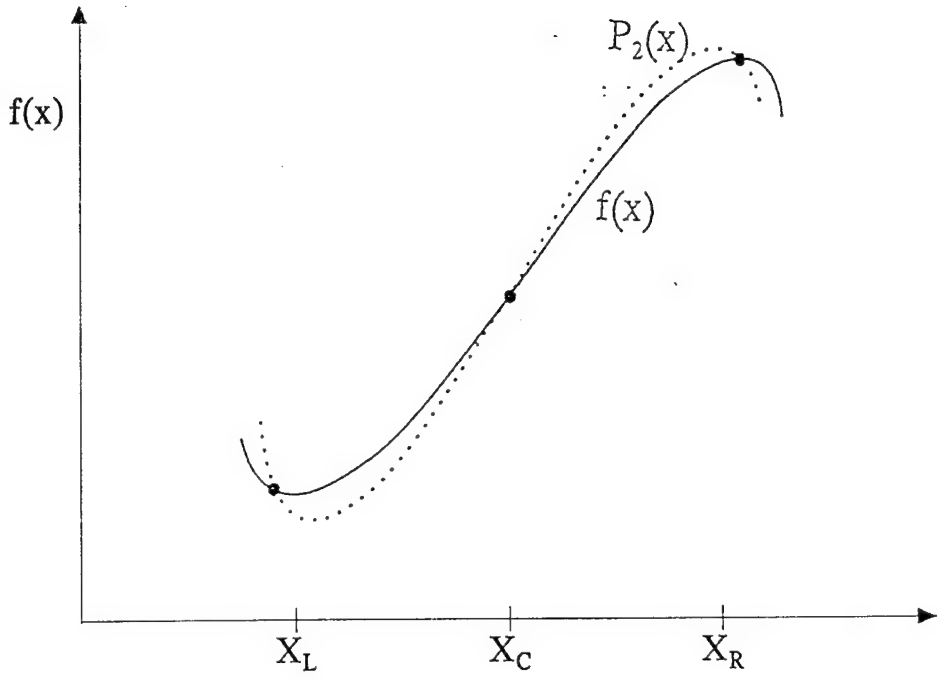

Fig. 5. Second degree Lagrangian interpolation function.

$$\frac{d^2 f(x)}{dx^2} = \frac{2f(x_L)}{(x_L - x_C)(x_L - x_R)} + \frac{2f(x_C)}{(x_C - x_L)(x_C - x_R)} + \frac{2f(x_R)}{(x_R - x_L)(x_R - x_C)} \tag{4}$$

Similar expressions for the derivatives with respect to y can be obtained.

The boundary conditions for the microstrip transmission lines shown in Figs. 1 to 4 are given by

$V = V_1$ on strip 1

$V = V_2$ on strip 2

$V = 0$ on the ground plane

$\oint_s \bar{D} \cdot \bar{ds} = 0$ on the dielectric interfaces

where V_1 and V_2 are arbitrary constant potentials and s is the closed surface around a grid point on the interface.

The last condition is based on Gauss's law for the electric field, i.e.

$$\oint_s \bar{D} \cdot \bar{ds} = \oint_s \epsilon \bar{E} \cdot \bar{ds} = Q_{enc} = 0 \tag{5}$$

where Q_{enc} is set to zero since no free charges exist on the dielectric boundaries. The surface integration in equation (5) can be replaced by a contour integration, because the microstrip transmission lines considered are two-dimensional structures, and the solution of the potential is independent of z [3].

Substituting $\bar{E} = -\nabla V$ in equation (5) yields :

$$\oint_{\ell} \epsilon \nabla V \cdot \hat{n}\, d\ell = \oint_{\ell} \epsilon \frac{\partial V}{\partial n} d\ell = 0 \tag{6}$$

where $\partial V/\partial n$ denotes the derivative of V normal to the contour ℓ, as shown in Fig. 6. It should be noted here that the normal is defined as the vector pointing out of the area enclosed by the contour ℓ. Figure 6 shows a general point (C) which is surrounded by four different dielectric materials, this is the most general case, and the mesh generator program provides the data about all these dielectric materials around such point. After applying equation (6) to the contour around that point, an expression is obtained for the computation of the voltage at these type of general points, that is

$$\begin{aligned} &-\frac{V_C}{2}\left[\left(\frac{(\epsilon_1+\epsilon_2)}{y_T-y_C}\right)-\left(\frac{(\epsilon_1+\epsilon_4)}{x_L-x_C}\right)-\left(\frac{(\epsilon_4+\epsilon_3)}{y_B-y_C}\right)+\left(\frac{(\epsilon_3+\epsilon_2)}{x_R-x_C}\right)\right] \\ &+\frac{V_T}{2}\left(\frac{(\epsilon_1+\epsilon_2)}{y_T-y_C}\right)-\frac{V_L}{2}\left(\frac{(\epsilon_1+\epsilon_4)}{x_L-x_C}\right)-\frac{V_B}{2}\left(\frac{(\epsilon_4+\epsilon_3)}{y_B-y_C}\right) \\ &+\frac{V_R}{2}\left(\frac{(\epsilon_3+\epsilon_2)}{x_R-x_C}\right)=0 \end{aligned} \tag{7}$$

The above equation deals with any kind of point because the permitivities of the regions around point C do not need to be all different. If all dielectric regions are the same then the point is in a homogeneous medium, and in inhomogeneous cases, the point will be located at a surface or line interface between two or three different media, respectively.

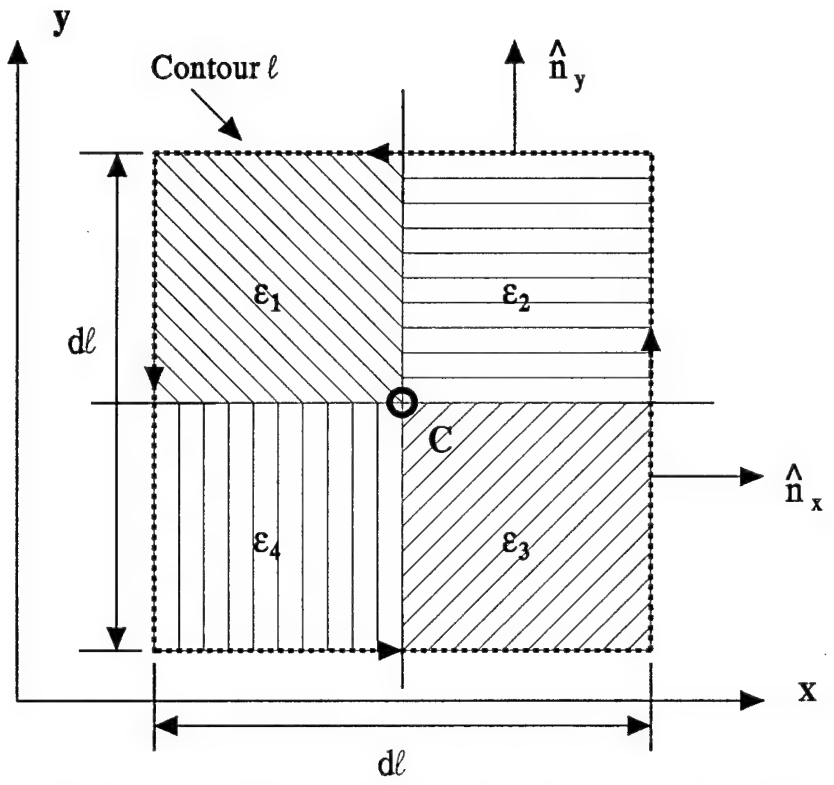

Fig. 6. Application of Gauss's law around a general point C located at the intersection between 4 different dielectrics.

B) Artificial Boundary Condition at the outer boundary

For the transmission lines shown in Figs. 1 to 4, approximate boundary conditions should be applied at the outer artificial boundary in order to truncate the mesh so that numerical analysis could be carried out. The equation used on the general type point (type *C*) can not be used here. The mesh generator program defines a new type for the points on the boundary, type "B", which is subdivided in subtypes depending on the location of the boundary point. At these points the approximate boundary condition proposed by Khebir et. al is used [4]. The series expansion for the electric potential is defined as [5]

$$V(\rho,\phi) = C_0 + A_0(\phi)\ln\rho + \sum_{n=1}^{\infty} \frac{A_n(\phi)}{\rho^n} \tag{8}$$

where the constant term, C_0, is dropped because the potential at infinity is zero. The second term in equation (8) is also dropped because the total charge enclosed by the mesh at the artificial boundary is also zero. Having set C_0 and A_0 to zero, equation (8) becomes

$$V(\rho,\phi) = \frac{A_1(\phi)}{\rho} + \frac{A_2(\phi)}{\rho^2} + \frac{A_3(\phi)}{\rho^3} + \cdots \tag{9}$$

Now, equation (9) is differentiated with respect to ρ , to obtain:

$$\frac{\partial V(\rho,\phi)}{\partial \rho} = -\frac{A_1(\phi)}{\rho^2} - \frac{2A_2(\phi)}{\rho^3} - \frac{3A_3(\phi)}{\rho^4} - \cdots \tag{10}$$

Then, multiply equation (9) by $1/\rho$ and add it to equation (10):

$$\frac{\partial V}{\partial \rho} + \frac{1}{\rho}V = \frac{A_1}{\rho^2} + \frac{A_2}{\rho^3} + \frac{A_3}{\rho^4} + \cdots - \frac{A_1}{\rho^2} - \frac{2A_2}{\rho^3} - \frac{3A_3}{\rho^4} - \cdots \tag{11}$$

Finally, rearranging equation (11) yields,

$$\frac{\partial V}{\partial \rho} + \frac{V}{\rho} = -\frac{A_2}{\rho^3} - \frac{2A_3}{\rho^4} - \frac{3A_4}{\rho^5} - \frac{4A_5}{\rho^6} - \cdots \tag{12}$$

As an approximation to equation (12), the right hand side is assumed to be zero. This truncation amounts to an error in the analysis which will be reduced as the value of ρ at the outer boundary is increased, i.e., as the outer boundary of the mesh is moved away from the strips.

The chain rule can be used to write $\partial V/\partial \rho$ as:

$$\frac{\partial V}{\partial \rho} = \frac{\partial V}{\partial x}\frac{\partial x}{\partial \rho} + \frac{\partial V}{\partial y}\frac{\partial y}{\partial \rho} \tag{13}$$

where $\rho(x,y) = \sqrt{x^2 + y^2}$. By dropping the right hand side of equation (12) and substituting the result into equation (13), one obtains

$$-\frac{V}{\rho} = \frac{\partial V}{\partial x}\frac{\partial x}{\partial \rho} + \frac{\partial V}{\partial y}\frac{\partial y}{\partial \rho} \tag{14}$$

Since $x = \rho \cos(\phi)$ and $y = \rho \sin(\phi)$, the derivatives of ρ with respect to x and y are thus defined as:

$$\frac{\partial x}{\partial \rho} = \cos(\phi) = \frac{x}{\rho} \quad , \quad \frac{\partial y}{\partial \rho} = \sin(\phi) = \frac{y}{\rho} \tag{15}$$

Substituting the results from equation (15) into equation (14) yields

$$-V = x\frac{\partial V}{\partial x} + y\frac{\partial V}{\partial y} \tag{16}$$

Equation (16) can be rewritten as

$$\frac{\partial V}{\partial x} = -\frac{1}{x}\left(V + y\frac{\partial V}{\partial y}\right) \tag{17}$$

Equation (17) can be implemented along the left and right boundaries of the mesh. Figure 7a shows the grid point system and the notations for boundary points. As an example, on the right boundary (type "B5" points) of the grid point C_5 resides on the boundary and R_5 is a point outside the outer boundary. Because R_5 lies outside the mesh, it is not possible to enforce Laplace's equation (1) at node C_5 in the usual manner. Instead, equation (17) is used to determine the potential at R_5, i.e. V_R, in terms of V_L, V_C, V_T, and V_B. Then, once V_R is known equation (1) can be enforced. The normal derivative of the potential at point C_5 on the right boundary is defined as

$$\frac{\partial V_C}{\partial x} = \frac{V_R - V_L}{x_R - x_L} = \frac{V_R - V_L}{2\Delta} \tag{18}$$

where $2\Delta = x_R - x_L$. By substituting the expression derived in equation (17) into equation (18), one obtains:

$$V_R = V_L - \frac{2\Delta}{x_C}\left(V_C + y_C\frac{\partial V_C}{\partial y}\right) \tag{19}$$

The term $\partial V_C/\partial y$ is then replaced by its finite difference approximation to give

$$V_R = V_L - \frac{2\Delta}{x_C}\left[V_C + y_C\left(\frac{(y_C-y_T)}{(y_B-y_C)(y_B-y_T)}V_B + \frac{(y_C-y_B)}{(y_T-y_B)(y_T-y_C)}V_T + \frac{(y_C-y_B)+(y_C-y_T)}{(y_C-y_B)(y_C-y_T)}V_C\right)\right] \tag{20}$$

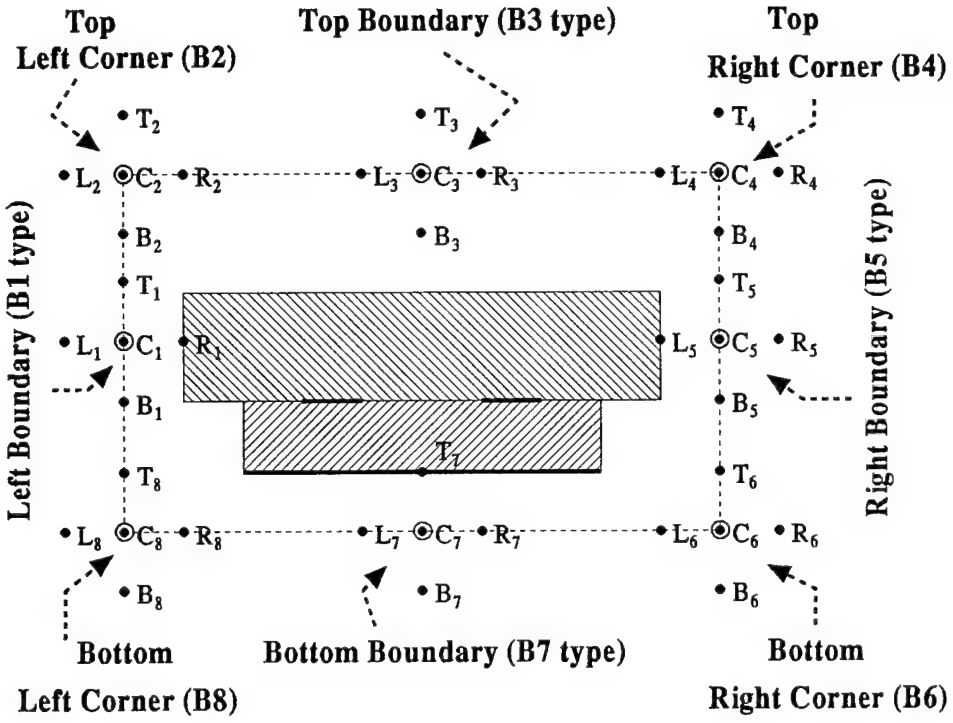

Fig. 7a. Artificial boundaries showing the points that lie outside of the FD mesh for each type of boundary and corner.

which can be rearranged to form

$$V_R = V_L + V_C\left[\frac{-2\Delta}{x_C}\left(1 + y_c\frac{(y_C-y_B)+(y_C-y_T)}{(y_C-y_B)\ (y_C-y_T)}\right)\right]$$

$$+ V_B\left[\frac{-2\Delta y_C}{x_C}\left(\frac{(y_C-y_T)}{(y_B-y_C)\,(y_B-y_T)}\right)\right] + V_T\left[\frac{-2\Delta y_C}{y_C}\left(\frac{(y_C-y_B)}{(y_T-y_B)\,(y_T-y_C)}\right)\right] \tag{21}$$

For simplicity, equation (21) can be written as:

$$V_R = C_L V_L + C_C V_C + C_B V_B + C_T V_T \tag{22}$$

where C_L , C_C , C_B , and C_T represent the coefficients of the potentials as defined in equation (21). Now that V_R is expressed in terms of V_L , V_C , V_B , and V_T , Laplace's equation, (1), can be used to relate the potential at the grid points on the boundary to their surrounding nodes. Applying equation (1) at node C_5 gives

$$K_R V_R + K_L V_L + K_T V_T + K_B V_B + K_C V_C = 0 \tag{23}$$

where

$$K_L = \frac{1}{(x_L-x_C)\,(x_L-x_R)} \quad , \quad K_R = \frac{1}{(x_R-x_L)\,(x_R-x_C)}$$

$$K_T = \frac{1}{(y_T-y_C)\,(y_T-y_B)} \quad , \quad K_B = \frac{1}{(y_B-y_C)\,(y_B-y_T)} \tag{24}$$

$$K_C = \frac{1}{(x_C-x_L)\,(x_C-x_R)} + \frac{1}{(y_C-y_T)\,(y_C-y_B)}$$

Substituting the expression for V_R in (22) in to (23) yields

$$V_L[K_R C_L + K_L] + V_C[K_R C_C + K_C] + V_B[K_R C_B + K_B] + V_T[K_R C_T + K_T] = 0 \qquad (25)$$

This is the equation that is enforced along the right side of the outer boundary. The method used along the left, top and bottom sides of the outer boundary is similar, as shown in Fig. 7a. Thus, on the left boundary (type "B1" points) we have

$$V_R[K_L C_R + K_R] + V_C[K_L C_C + K_C] + V_B[K_L C_B + K_B] + V_T[K_L C_T + K_T] = 0 \qquad (26)$$

where

$$\left.\begin{aligned} C_R &= 1 \\ C_C &= \left[\frac{2\Delta}{x_C}\left(1 + y_C\frac{(y_C - y_B) + (y_C - y_T)}{(y_C - y_B)\,(y_C - y_T)}\right)\right] \\ C_B &= \left[\frac{2\Delta y_C}{x_C}\left(\frac{(y_C - y_T)}{(y_B - y_C)\,(y_B - y_T)}\right)\right] \\ C_T &= \left[\frac{2\Delta y_C}{y_C}\left(\frac{(y_C - y_B)}{(y_T - y_B)\,(y_T - y_C)}\right)\right] \end{aligned}\right\} \qquad (27)$$

and K_L, K_R, K_C, K_T, and K_B are defined in equation (24).

In order to apply the same numerical procedure on the top side of the outer boundary, equation (17) should be rewritten as

$$\frac{\partial V}{\partial y} = -\frac{1}{y}\left(V + x\frac{\partial V}{\partial x}\right) \qquad (28)$$

Starting from equation (28), the same analysis, as for the left side, is repeated to obtain an expression for the top side (type "B3" points) as

$$V_B[K_TC_B + K_B] + V_C[K_TC_C + K_C] + V_R[K_TC_R + K_R] + V_L[K_TC_L + K_L] = 0 \qquad (29)$$

where

$$\left.\begin{aligned} C_B &= 1 \\ C_C &= \left[\frac{-2\Delta}{y_C}\left(1 + x_C\frac{(x_C - x_L) + (x_C - x_R)}{(x_C - x_L)\,(x_C - x_R)}\right)\right] \\ C_R &= \left[\frac{-2\Delta x_C}{y_C}\left(\frac{(x_C - x_L)}{(x_R - x_L)\,(x_R - x_C)}\right)\right] \\ C_L &= \left[\frac{-2\Delta x_C}{y_C}\left(\frac{(x_C - x_R)}{(x_L - x_C)\,(x_L - x_R)}\right)\right] \end{aligned}\right\} \qquad (30)$$

and again K_L, K_R, K_C, K_T, and K_B are defined in equation (24). From equation (28) and following the same procedure, an expression is obtained for the lower boundary ("B7" type points)

$$V_T[K_BC_T + K_T] + V_C[K_BC_C + K_C] + V_R[K_BC_R + K_R] + V_L[K_BC_L + K_L] = 0 \qquad (31)$$

where

$$\left.\begin{aligned} C_T &= 1 \\ C_C &= \left[\frac{+2\Delta}{y_C}\left(1 + x_C\frac{(x_C - x_L) + (x_C - x_R)}{(x_C - x_L)\,(x_C - x_R)}\right)\right] \\ C_R &= \left[\frac{+2\Delta x_C}{y_C}\left(\frac{(x_C - x_L)}{(x_R - x_L)\,(x_R - x_C)}\right)\right] \\ C_L &= \left[\frac{+2\Delta x_C}{y_C}\left(\frac{(x_C - x_R)}{(x_L - x_C)\,(x_L - x_R)}\right)\right] \end{aligned}\right\} \qquad (32)$$

where Δ is defined as $\Delta = (y_T - y_C)$. Again these coefficients must be substituted in the general equation to obtain an expression for the points on the lower boundary. At the four corners of the artificial boundary (types B2, B4, B6, and B8), another procedure is used. Figure 7b shows a sketch of these corners and the neighboring nodes. For example, at right upper corner, the potential at C will be related to the potential at the left, V_L and at the bottom, V_B. Because equation (12) is based on the first order expansion of equation (9), the potential at the corners will also be related to only $1/\rho$. Thus $A_1(\phi) = \rho\, V(\rho,\phi)$. Using linear interpolation, the value of A_1 at ϕ_C can be related to its value at ϕ_B and ϕ_L as

$$A_1(\phi_C) = A_1(\phi_B) + \frac{A_1(\phi_L) - A_1(\phi_B)}{\phi_L - \phi_B}(\phi_C - \phi_B) \qquad (33)$$

If $A_1(\phi) = \rho\, V(\rho,\phi)$ is substituted in equation (33), one obtains

$$\rho_C V_C = \rho_B V_B + \frac{\rho_L V_L - \rho_B V_B}{\phi_L - \phi_B}(\phi_C - \phi_B) \qquad (34)$$

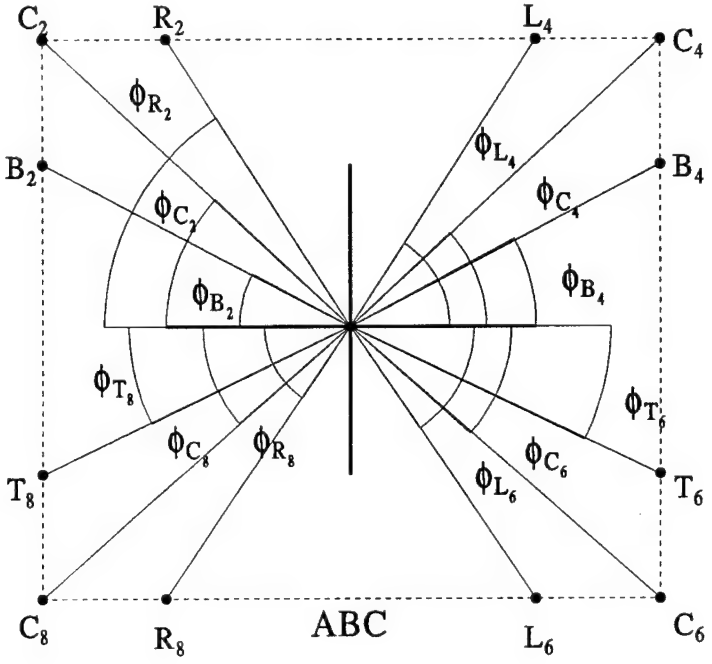

Fig. 7b. Artificial boundaries showing points at the corners and points on the boundary from which the potential at C_n may be computed by interpolation.

Now, equation (34) can be rearranged to obtain

$$V_C \rho_C + V_B\left(-\rho_B + \rho_B\frac{\phi_C - \phi_B}{\phi_L - \phi_B}\right) + V_L\left(-\rho_L\frac{\phi_C - \phi_B}{\phi_L - \phi_B}\right) = 0 \qquad (35)$$

where

$$\rho = \sqrt{x^2 + y^2} \quad , \quad \phi = \tan^{-1}\left(\frac{y}{x}\right) \qquad (36)$$

At the left upper corner, the same analysis can be repeated to yield:

$$V_C \rho_C + V_R\left(-\rho_R + \rho_R\frac{\phi_C - \phi_R}{\phi_B - \phi_R}\right) + V_B\left(-\rho_B\frac{\phi_C - \phi_R}{\phi_B - \phi_R}\right) = 0 \qquad (37)$$

Then it can be applied to the lower left and right corners where the following expressions are obtained,

$$V_C \rho_C + V_R\left(-\rho_R + \rho_R\frac{\phi_C - \phi_R}{\phi_T - \phi_R}\right) + V_T\left(-\rho_T\frac{\phi_C - \phi_R}{\phi_T - \phi_R}\right) = 0 \qquad (38)$$

for the lower left, and for the lower right corner

$$V_C \rho_C + V_L\left(-\rho_L + \rho_L\frac{\phi_C - \phi_L}{\phi_T - \phi_L}\right) + V_T\left(-\rho_T\frac{\phi_C - \phi_L}{\phi_T - \phi_L}\right) = 0 \qquad (39)$$

C) Construction of the Matrix Equation.

The equations derived above, describe the potential at a node by relating it to the potential at neighbor nodes in the mesh. Therefore, application of those equations at all the nodes in the mesh leads to a set of simultaneous equations that can be described as the matrix equation $[A][X] = [B]$. This matrix equation is like the one found in [6]. The Matrix $[A]$

is diagonally dominant with the elements away from the diagonal being zeros. Therefore, [*A*] is a banded matrix, and, like in [6], it is desirable to take advantage of this fact when solving the system of equation. Linpack Subroutines [7], SGBCO and SGBSL are used to solve for the potential distribution on the mesh, the column vector [*X*]. Once the potential is known for every node on the FD mesh then the characteristic parameters of the transmission line can be determined.

CHAPTER III

COMPUTATION OF THE TRANSMISSION LINE PARAMETERS

A) Introduction

After solving Laplace's equation, the potential distribution on the FD mesh is known. From the potential distribution the electric fields on the mesh may be computed. The characteristics of the transmission line may also be computed from the potential distribution [6].

B) Computing the Electric Field Vectors at the Mesh Points

Once the potential distribution on the mesh has been computed, the field distribution inside the FD mesh domain can be found. The derivation starts from the following definition

$$\boldsymbol{E} = -\nabla V \tag{40}$$

where at any node we get

$$\boldsymbol{E}_x = -\frac{\partial V}{\partial x}\,\hat{\boldsymbol{a}}_x \quad , \quad \boldsymbol{E}_y = -\frac{\partial V}{\partial y}\,\hat{\boldsymbol{a}}_y \tag{41}$$

then the finite difference approximation given by (2) and (3) is used to obtain the electric field components at any mesh point inside the FD mesh domain, i.e.

$$E_x = -\frac{(x_C - x_R)}{(x_L - x_C)(x_L - x_R)} V_L - \frac{(x_C - x_L) + (x_C - x_R)}{(x_C - x_L)(x_C - x_R)} V_C - \frac{(x_C - x_L)}{(x_R - x_L)(x_R - x_C)} V_R \tag{42}$$

$$E_y = -\frac{(y_C - y_T)}{(y_B - y_C)(y_B - y_T)} V_B - \frac{(y_C - y_B) + (y_C - y_T)}{(y_C - y_B)(y_C - y_T)} V_C - \frac{(y_C - y_B)}{(y_T - y_B)(y_T - y_C)} V_T \tag{43}$$

C) Computation of Total Charge

To find the characteristic impedance and the phase velocities for a transmission line having an inhomogeneous medium requires calculating the capacitances of the structure, with and without the dielectric regions [8]. Since the capacitance per unit length is directly related to the charge per unit length on the strips, the problem is reduced to finding the total charge per unit length on the strips. The microstrip transmission lines shown in Figs. 1 to 4 have two horizontal conductors placed between the two dielectric regions. It will be assumed throughout the analysis of the problem that the conductors employed are perfectly conducting strips. It will also be assumed that the dielectric materials are to be lossless, isotropic, and homogeneous. Let Q^i denote the total charge on the i^{th} conductor. If Gauss' law is applied to a closed path ℓ enclosing the i^{th} conductor, the total charge on that conductor is then expressed as:

$$\oint_s \bar{D} \cdot \bar{ds} = \oint_s \epsilon \bar{E} \cdot \bar{ds} = Q^i_{enc} \tag{44}$$

where $\bar{D}$ is the displacement vector and ds is the elemental area. Substituting for $\bar{E} = -\nabla V$ in equation (44) yields

$$-\oint_s \epsilon \nabla V \cdot \hat{n}\, ds = -\oint_\ell \int_0^g \epsilon \frac{\partial V}{\partial n} dz\, d\ell = Q^i_{enc} \tag{45}$$

The integrand in equation (45) is independent of z, and hence the integral along the z-axis is a constant. The total charge per unit length is then given from equation (45) as

$$\frac{Q^{i}_{enc}}{g} = -\oint_{\ell} \epsilon \frac{\partial V}{\partial n} d\ell \tag{46}$$

The contour ℓ surrounds the i^{th} conductor, and it can be explicitly prescribed on the four sides surrounding the conductor; thus

$$\frac{Q^{i}_{enc}}{g} = -\left[\int_{RS} \epsilon(x,y)\frac{\partial V}{\partial x}dy + \int_{TS} \epsilon(x,y)\frac{\partial V}{\partial y}dx + \int_{LS} \epsilon(x,y)\frac{\partial V}{\partial x}dy + \int_{BS} \epsilon(x,y)\frac{\partial v}{\partial y}dx\right] \tag{47}$$

where the notation *RS*, *TS*, *LS*, and *BS* stands for the right, top, left, and bottom sides, respectively. The parameter g is the length of the transmission line along the z direction. To further illustrate how equation (47) is applied, consider the grid points shown in Fig.8. For simplicity, the charge along the top and bottom sides will only be expanded assuming for a few grid points on the contour around the strip. Applying (46) on the right and top side yields

$$\begin{aligned} Q^{i}_{TS} = {} & \frac{\epsilon_1}{2}\left[\left(\frac{(V_3-V_1)}{(y_3-y_1)} + \frac{(V_6-V_4)}{(y_6-y_4)}\right)(x_2-x_5) + \left(\frac{(V_9-V_7)}{(y_9-y_7)} + \frac{(V_6-V_4)}{(y_6-y_4)}\right)(x_5-x_8)\right] \\ & + \frac{\epsilon_1}{2}\left[\left(\frac{(V_{12}-V_{10})}{(y_{12}-y_{10})} + \frac{(V_9-V_7)}{(y_9-y_7)}\right)(x_8-x_{11}) + \left(\frac{(V_{15}-V_{13}}{(y_{15}-y_{13})} + \frac{(V_{12}-V_{10})}{y_{12}-y_{10})}\right)(x_{11}-x_{14})\right] \end{aligned} \tag{48}$$

$$Q^{i}_{RS} = \frac{\epsilon_2}{2}\left[\left(\frac{(V_3-V_1)}{(x_3-x_1)} + \frac{(V_6-V_4)}{(x_6-x_4)}\right)(y_5-y_2)\right] + \frac{\epsilon_1}{2}\left[\left(\frac{(V_6-V_4)}{(x_6-x_4)} + \frac{(V_9-V_7)}{(x_9-x_7)}\right)(y_8-y_5)\right] \tag{49}$$

and on the left and bottom sides,

$$Q^{i}_{LS} = \frac{\epsilon_2}{2}\left[\left(\frac{(V_1-V_3)}{(x_3-x_1)} + \frac{(V_4-V_6)}{(x_6-x_4)}\right)(y_5-y_2)\right] + \frac{\epsilon_1}{2}\left[\left(\frac{(V_4-V_6)}{(x_6-x_4)} + \frac{(V_7-V_9)}{(x_9-x_7)}\right)(y_8-y_5)\right] \tag{50}$$

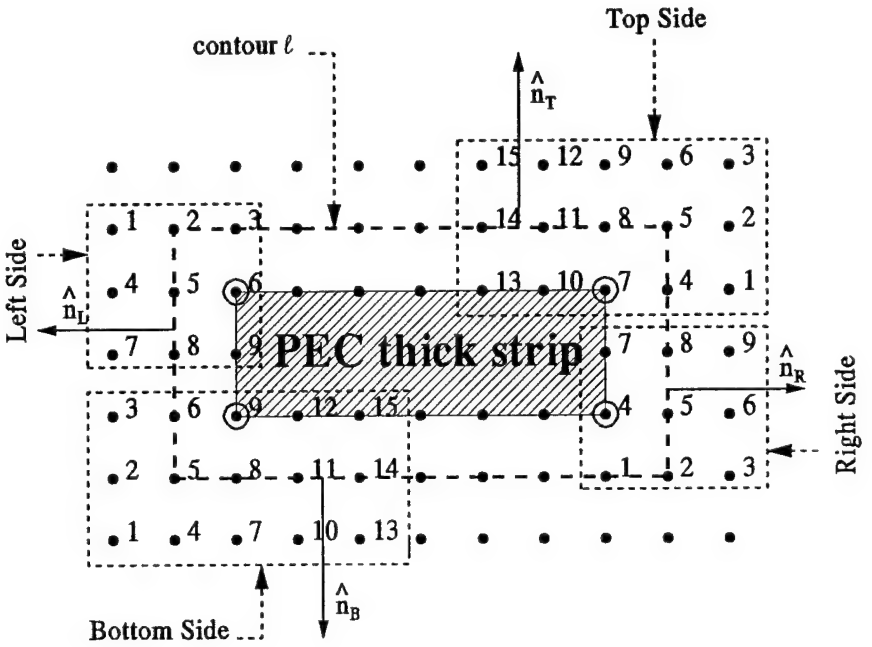

Fig. 8. The FD mesh around the strip and the labeling of the points for the application of Gauss's law on the four sides of contour ℓ in order to compute the total charge on the strip.

$$Q_{BS}^{i} = \frac{\epsilon_2}{2}\left[\left(\frac{(V_1-V_3)}{(y_3-y_1)}+\frac{(V_4-V_6)}{(y_6-y_4)}\right)(x_5-x_2)+\left(\frac{(V_7-V_9)}{(y_9-y_7)}+\frac{(V_4-V_6)}{(y_6-y_4)}\right)(x_8-x_5)\right]$$
$$+\frac{\epsilon_2}{2}\left[\left(\frac{(V_{10}-V_{12})}{(y_{12}-y_{10})}+\frac{(V_7-V_9)}{(y_9-y_7)}\right)(x_{11}-x_8)+\left(\frac{(V_{13}-V_{15}}{(y_{15}-y_{13})}+\frac{(V_{10}-V_{12})}{y_{12}-y_{10})}\right)(x_{14}-x_{11})\right] \quad (51)$$

where the total charge per unit length on the i^{th} conductor is then described as:

$$\frac{Q_{enc}^{i}}{g} = -\left[Q_{RS}^{i}+Q_{TS}^{i}+Q_{LS}^{i}+Q_{BS}^{i}\right], \qquad i=1,2 \quad (52)$$

D) Computation of Self and Mutual Capacitances, Impedances, Phase Velocities and Coupling Coefficients

Following the same procedures presented in [1] and [6], the characteristics of the transmission lines are computed. In the previous section it was shown how the total charge on each conductor may be computed. From the total charge and the voltage on each conducting strip, the self and mutual capacitances are found for the given transmission line. From the total charges, the effective permitivities for all the modes (odd or even for the two conductor case) are computed, and with them the phase velocities are found. With the phase velocities, and the self and mutual capacitances the characteristic impedance of the line is computed. For the two conductor case, the odd and even impedances are found, and from them, the characteristic impedance for the two conductor line is computed.

If a voltage V_1 on one conductor, excites a voltage V_2 on the other conductor, then the electric coupling $k_e = V_2/V_1$ [7]. which may be written in terms of the capacitances as

$$k_{e12} = 20 \log_{10}\left[\frac{C_{12}}{C_{11} + C_{12}}\right] \tag{53}$$

But if there is a voltage V_2 on the second conductor, the one that excites a voltage V_1 on the first conductor then the coupling equation is defined as

$$k_{e21} = 20 \log_{10}\left[\frac{C_{21}}{C_{22} + C_{12}}\right] \tag{54}$$

For a symmetric microstrip transmission line, $C_{11} = C_{22}$, $C_{12} = C_{21}$, and therefore $k_{e12} = k_{e21} = k_e$. so the above equations for the capacitive coupling yield the same result.

CHAPTER IV
NUMERICAL RESULTS AND DISCUSSION

A) Introduction

This section presents the results obtained from analyzing a series of geometries. Two different FORTRAN codes are developed. The first, generates the FD mesh. The second solves for the potential distribution and computes the line parameters. In this section, the creation of an input file for the mesh generator is presented. Then, some results are compared with previously published data. Finally, the effect of the air gap is shown for the geometries shown in Figs. 1 to 4.

B) Generating the FD Mesh

A mesh generator program was created to make it easy to build FD Meshes for a number of geometries by writing an input file that defines the geometry. To show the way such file is created, the steps needed will be followed for a sample geometry. The geometry chosen is shown in Fig. 9. The starting point for the input data file should be a sketch of the cross section of the transmission line to be analyzed (see Figs. 1 to 4 and 9.) The dimensions should all be known as well as the permitivities of the materials. The conductors on this geometries are assumed to be perfect electric conductors (PECs). An Artificial Boundary (ABC) at which the mesh will be truncated is chosen. The procedure is the same as that in a SPICE netlist where a circuit is described by defining a number of nodes and then the different elements between them and, in this case, the mesh generator input file consisting of a series of blocks, their position, and material is defined. There is an important rule when defining these blocks, that is, it must have only one kind of dielectric material, or a PEC. The different blocks or cells on which the cross section of the transmission line has been subdivided are shown in Fig. 10. The Input Data File follows the following format. The first line of the file is a text line describing the geometry, and the next two lines contain the number of blocks on the x and y directions. The next set of lines indicate how many points or nodes the user wants on each block.

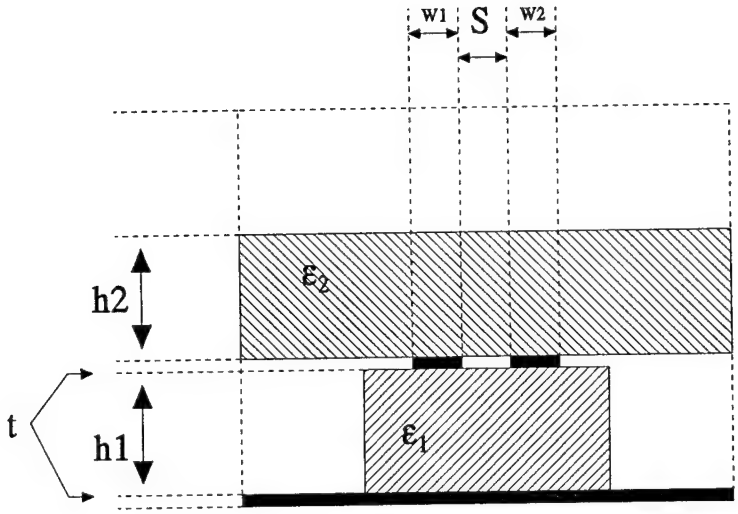

Fig. 9.Relation between dimensions of the transmision line and values of the relative permitivities used in obtaining numerical results. t/h1 = 0.01, h1=h2, s/h1=.5, W1=W2, W1/h1 = 0.5, ε_1 = 2.25, 4.8, 9.6, ε_2=2.25,4.8,9.6, and, 1.0 (no overlay).

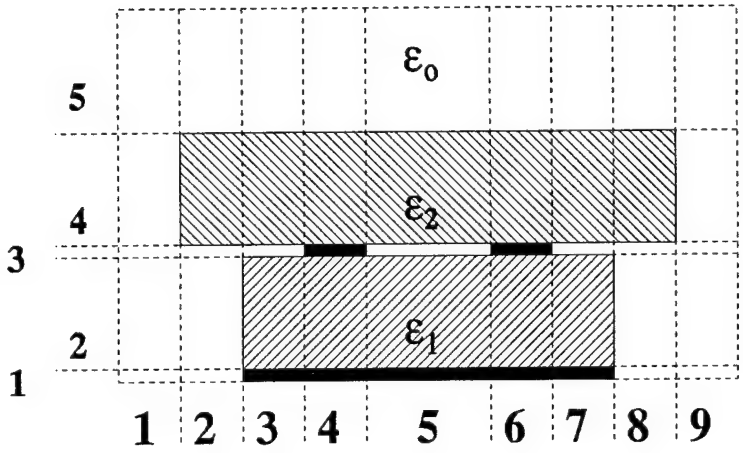

Fig.10. An x-y plane cut showing the block structure to set up the input file for the mesh generator program.

This allows the program to generate, non uniform meshes. The input data file appears as follows:

Line #1	Two striplines w/ dielectric substrate and overlay (Fig. 1.)	
Line #2	9	!Number of blocks on x direction
Line #3	5	!Number of blocks on y direction
Line #4	1	!No. of points in the first block in the x direction
Line #5	2	
Line #6	2	
Line #7	3	
Line #8	5	
Line #9	3	
Line #10	2	
Line #11	2	
Line #12	1	!No. of points in the last block (#9) in the x direction
Line #13	2	!No. of points in the first block in the y direction
Line #14	3	
Line #15	2	
Line #16	3	
Line #17	1	!No. of points in the last block (#5) in the y direction

This file must contain some information about the material and position of each block where the next set of lines are used to represent material characteristics. The first line of this set is a comment text line. This line acts as a remainder of how the next set of lines should be written. The lines after the comment, contain a set of integer and real numbers which contain all the information about a given block. Each of these lines defines a single block. For each line, the following information must be entered: the block index numbers (used for identification of the block), the lower left and upper right corners of the block, the relative permitivity of the block (the value 0.0 is used to indicate PEC), and the potential for a PEC block (dielectric blocks do not need to have a fixed potential specified so 0.0 may be entered in those cases). An example input for Fig. 10. is as follows:

Line #18	Block # i	Block # j	xlow	ylow	xup	yup	epsr	volt
Line #20	1	1	0.	0.	1.	0.5	1.	0.
Line #21	3	2	2.	0.5	3.	2.5	4.4	0.

```
Line #22      4        3        3.   2.5   4.   3.      0.0   5.   !PEC strip
.
.
.
Last Line  END                   ! last line
```

The blocks do not need to be put in any specific order since the indexes of the block describe its location on the cross section of the transmission line. Choosing some kind of order, however, makes debugging easier. The output file from this program contains all the information about the geometry in a series of points or nodes. To be more precise, it contains: the i and j indexes for each point; its x and y coordinates; the type of point, (general, boundary, and fixed as described in Chapter II); the permitivities of the four regions around each point (see Fig. 6.) or the voltage at the point in case of fixed potential points (i.e. points on the strips or the ground plane).

C) Comparison of Numerical Results with Previously Published Data

Before analyzing any of the geometries shown in Figs. 1 to 4, it is desirable to insure that the developed code is working properly. To accomplish this, the simple geometry found in Fig. 3 of [10] was analyzed for a series of dimensions. This geometry is a two conductor microstrip line with no overlay, i. e. ε_2 is set to 1, free space, and ε_1 is set to 9.6, Al_2O_3. The effective permitivities and the characteristic impedance of the line where computed for different dimensions, special care was taken in changing the number of points per block. By doing so, the separation of the nodes in the meshes was kept constant for all the dimensions. The output data obtain from the program was compared with the results from the program described in [10]. Table I and II contain these results.

Table I. Comparison of the results from the FD code for the characteristic impedances for the even and odd modes with the results given by Smith, et al. in [10]

Dimensions		Present		Reference [10]		%error	
s/h	w/h	Z_e	Z_o	Z_e	Z_o	Z_e	Z_o
0.5	0.5	85.97	46.88	83.78	49.85	2.6	5.9
1	1	57.14	42.68	56.25	42.85	1.5	0.3
2	2	35.64	32.39	35.59	32.08	0.14	0.96
1	0.5	78.51	56.18	76.92	57.03	2	1.5
0.5	1	61.3	36.65	60.22	37.67	1.7	2.7
1	0.2	104.84	73.61	103	77.35	1.7	4.8

Note: all the Impedances are expressed in Ohms

Table II. Comparison of the results from the FD code for the effective permitivities for the even and odd modes with the results given by Smith, et al. in [10]

Dimensions		Present		Reference [10]		%error	
s/h	w/h	$\varepsilon_{eff\ even}$	$\varepsilon_{eff\ odd}$	$\varepsilon_{eff\ even}$	$\varepsilon_{eff\ odd}$	$\varepsilon_{eff\ even}$	$\varepsilon_{eff\ odd}$
0.5	0.5	6.55	5.15	6.6	5.46	0.75	5.6
1	1	6.95	5.62	6.99	5.76	0.57	2.4
2	2	7.19	6.39	7.38	6.38	2.6	0.15
1	0.5	6.6	5.36	6.61	5.56	0.15	3.6
0.5	1	6.95	5.38	6.99	5.61	0.57	4.1
1	0.2	6.29	5.18	6.31	5.45	0.32	4.9

As seen from these two tables the results given by the FD analysis are close to those reported in [10]. The main difference between the transmission line analyzed in [10] and the one analyzed using the FD code is the thickness of the conductors. While [10] assumes conductors with no thickness, the FD analysis assumes conductors of thickness so that t/h1 = 0.01. For all the different dimensions analyzed, h1 remained equal to 1 unit and t was set to 0.01 units (see Fig. 9) and for these different cases only W1, W2 and S are changed. For

the case where s/h = W/h = 0.5, the number of points on the mesh was increased. Figure 11 shows the results of these computations, in which the convergence the effective permitivity and the characteristic impedance is very satisfactory.

Another geometry that was analyzed is the one given in Fig. 9 of [11]. This geometry consists of two microstrips with a groove etched between them. On Fig. 11 of [11], the characteristic impedance for the even and odd cases is plotted versus the depth of the groove (h_1) at 94GHz. From that figure data is obtained for case where h_1 = 50.0 μm. Table III shows the results obtained using the FD quasi-static technique used in this paper and the results presented in [11].

Table III. Comparison of results from the FD code for the characteristic impedances for the odd and even modes with the results reported in [11]

	Present	Reference [11]
Z_o	43.9Ω	40.5Ω
Z_e	51.38Ω	54Ω

D) The Effect of the Air Gap for the Large Overlay Geometry

In the previous section it was shown that the output from the program agrees with previously published data. Now the effect of the air gap was studied. The geometry with the large dielectric overlay (see Figs. 1 and 3) was analyzed for the dimensions given in Fig. 9. Different values of permitivities for both the substrate and the overlay were used. The code must first solve for the potential distribution on the mesh before computing all the line parameters. The different potential distributions for the odd mode for the geometries shown in Figs. 1 and 3 are shown on Fig. 12a. The dimensions are those given in Fig. 9, the permitivities are set so that ε_{r1} = 9.6 and ε_{r2} = 4.8. It is clear from Fig. 12a that the potential on the strips is fixed to 1 volt or -1 volt. The ground plane is clearly seen set to zero potential. It is also clear that the chosen ABC is working properly. There is not a clear difference between the potential distribution for the geometry with an air gap present (Fig. 1) and the

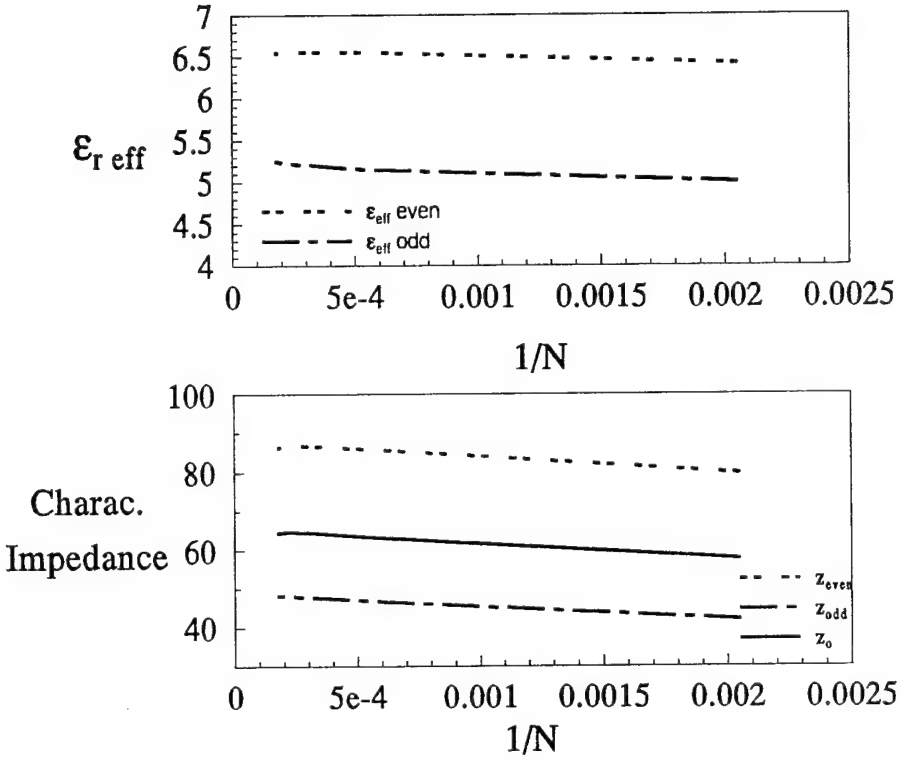

Fig.11. Convergence plot with no overlay, $\varepsilon_{r1} = 9.6$, $\varepsilon_{r2} = 1$, W1=W2, and S/h1 = W1/h1 = 0.5.

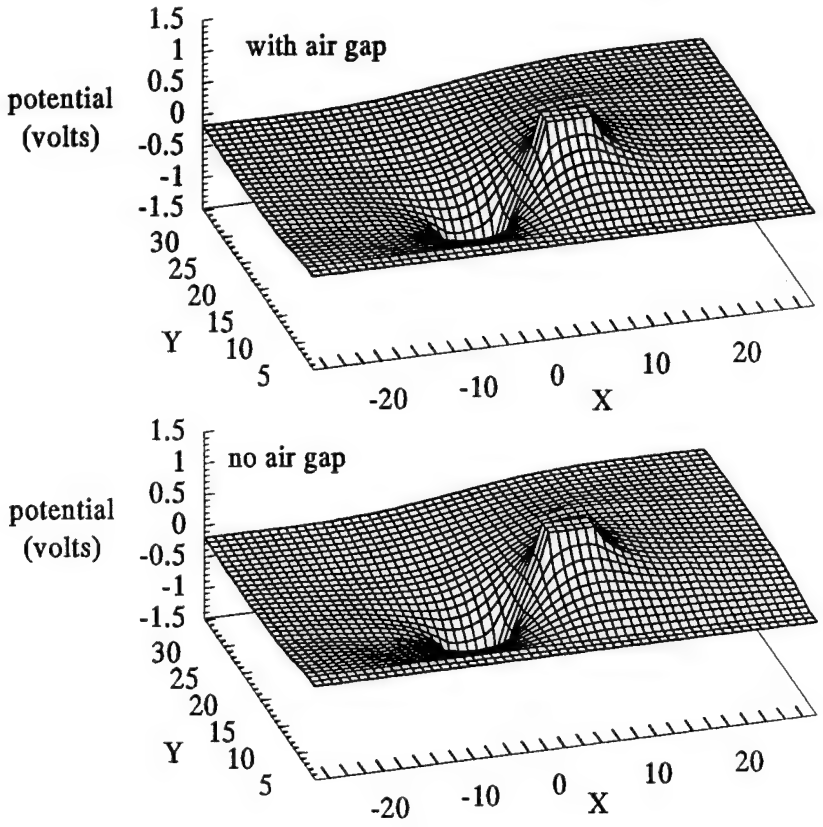

Fig. 12a. Potential distribution on the FD mesh for
$\varepsilon_{r1} = 9.6$, $\varepsilon_{r2} = 4.8$, $V_1 = -1$ Volt, and $V_2 = 1$ Volt.

one without one (Fig. 3). The potential distributions for the even mode are shown on Fig 12b. The strips with their potential fixed at 1 volt are easily identified. The ground plane set at zero volts is also clear. Right above the strips the interface between the overlay and the free space on top of it can be seen. The difference between the case with an air gap and without air gap is a little more clear than in the odd mode. The potential at a point between the strips is lower when the air gap is present. For this same case the number of nodes on the mesh was increased to check the stability of the code. Fig. 13 shows the convergence of the capacitive coupling and the self and mutual capacitances, that are equal for a symmetric geometry. Now for the geometries shown on Fig. 1 and 3, the permitivity of the substrate was left constant and the permitivity of the overlay was changed. Figs. 14a to 14c show the capacitive coupling and the mutual and self capacitances as a function of the overlay permitivity. For all the cases, the presence of the air gap reduces the capacitive coupling since the capacitance between the strips is reduced. The electric field distribution in the mesh is also obtained. Figures 15a to 15d show the vector field distribution for the even mode, with and without the air gap. Looking at the entire mesh, it does not appear to be any difference on the distribution of the electric field. Figures 15b and 15d show the area between the conductors, here the effect of the air gap is clearly seen. Figures 16a to 16d show the distribution for the odd mode. Again no effect is seen when the distribution on the whole mesh is studied. The details of the area between the conductors (Figs. 16b and 16c) show a small effect on the electric field, but not as big as the one for the even mode (Figs. 15b and 15d).

E) The Small Overlay Geometry

The small overlay geometry shown on Figs. 2 and 4 has also been analyzed. The dimensions used were those of a real microstrip transmission line that was used as a probe to measure the relative permitivity of unknown materials. The probe has the following dimensions; the width of both conductors is 4mm, separated by 2.5mm, while their thickness was calculated from the manufacturers specification of the amount of copper per square inch. The calculations yield 0.07112mm, and the same thickness was use to represent the ground

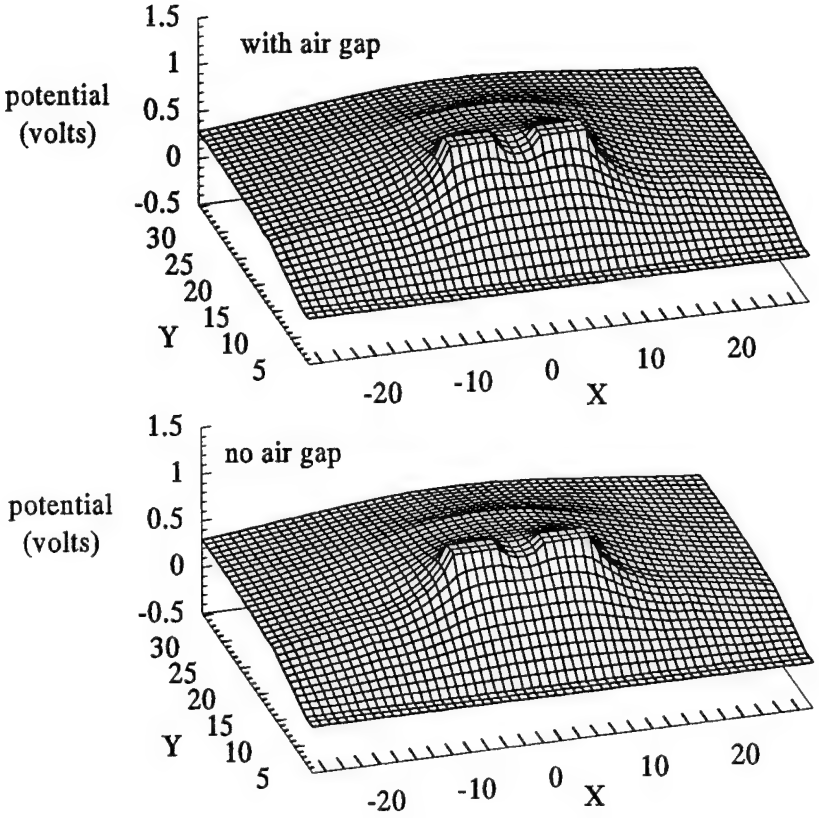

Fig. 12b. Potential distribution on the FD mesh for $\varepsilon_{r1} = 9.6$, $\varepsilon_{r2} = 4.8$, and $V_1 = V_2 = 1$ Volt.

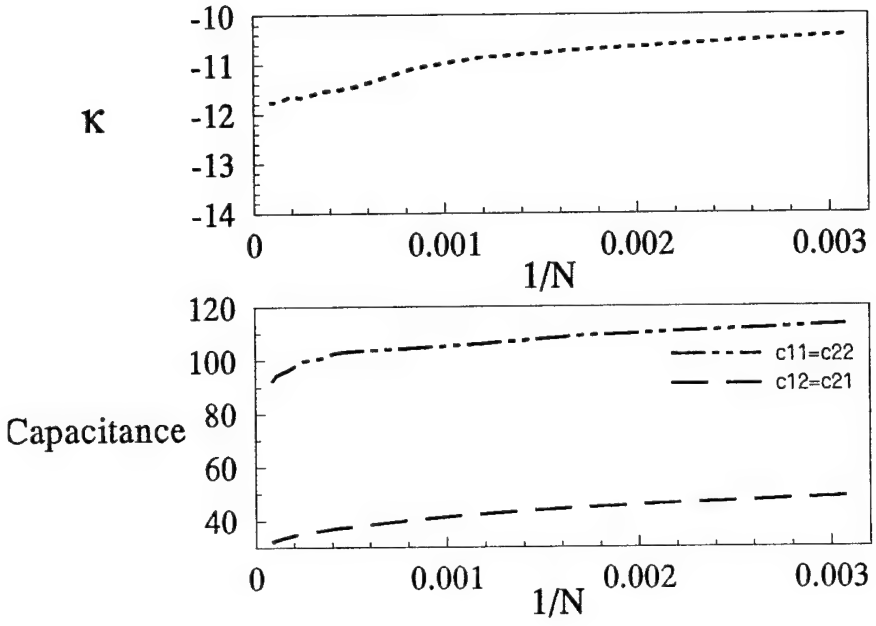

Fig. 13. Convergence of κ and the self and mutual capacitance for the large overlay geometry $\varepsilon_{r1} = 9.6$, $\varepsilon_{r2} = 4.8$ and with an air gap.

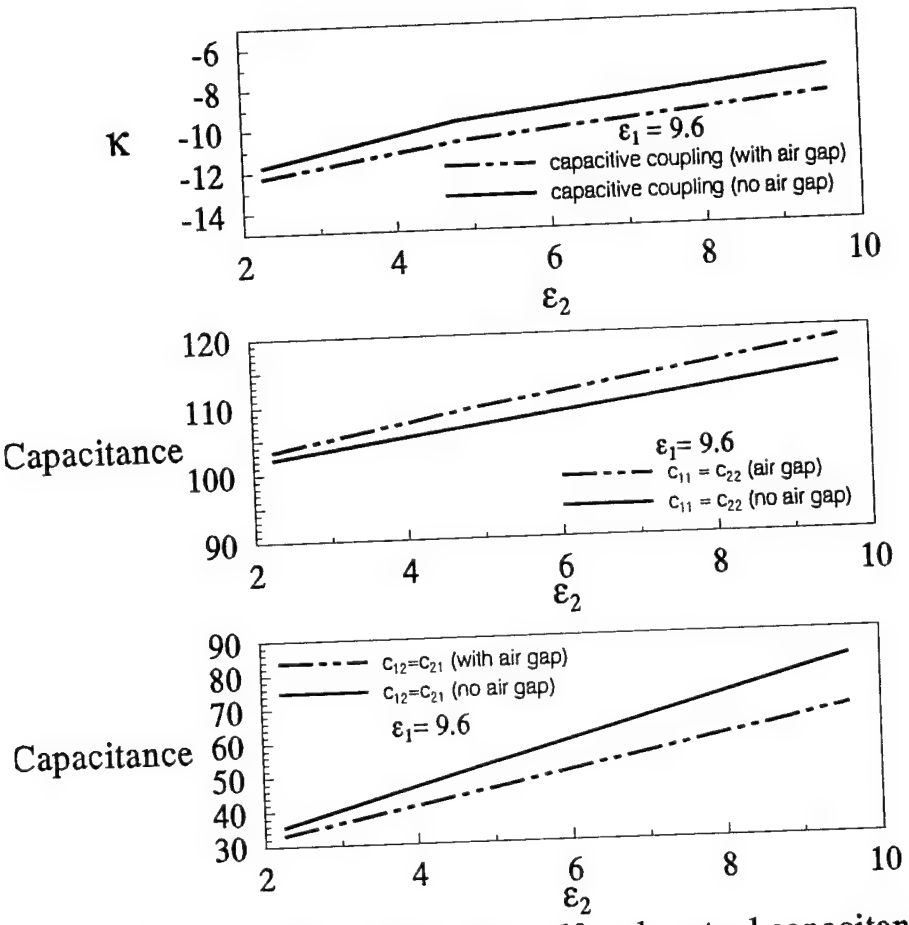

Fig. 14a. Coupling coefficient, self and mutual capacitances for different overlays, with and without air gap with $\varepsilon_{r1} = 9.6$.

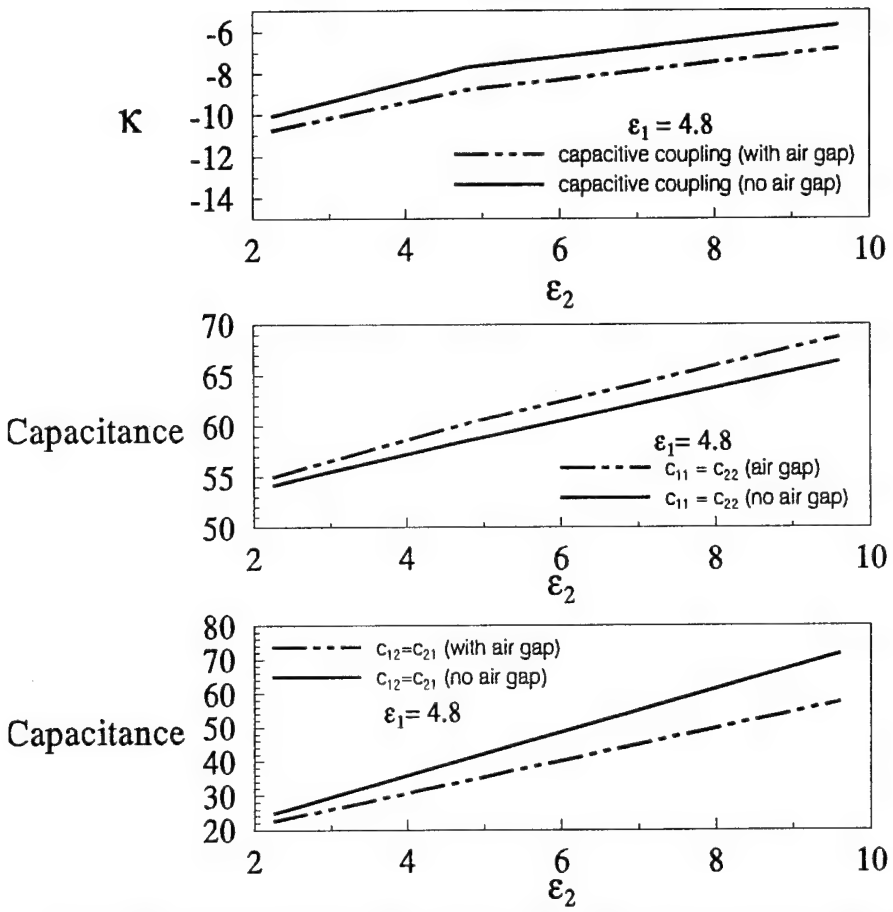

Fig. 14b. Coupling coefficient, self and mutual capacitances for different overlays, with and without air gap with $\varepsilon_{r1} = 4.8$

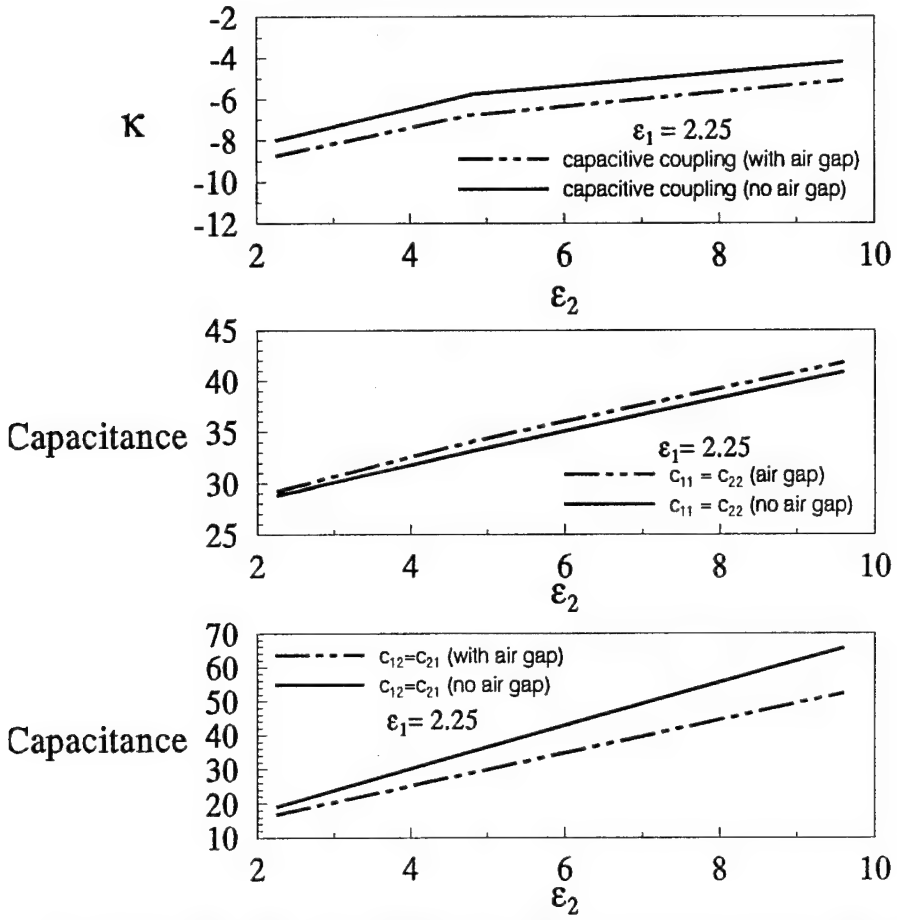

Fig. 14c. Coupling coefficient, self and mutual capacitances for different overlays, with and without air gap with $\varepsilon_{r1} = 2.25$.

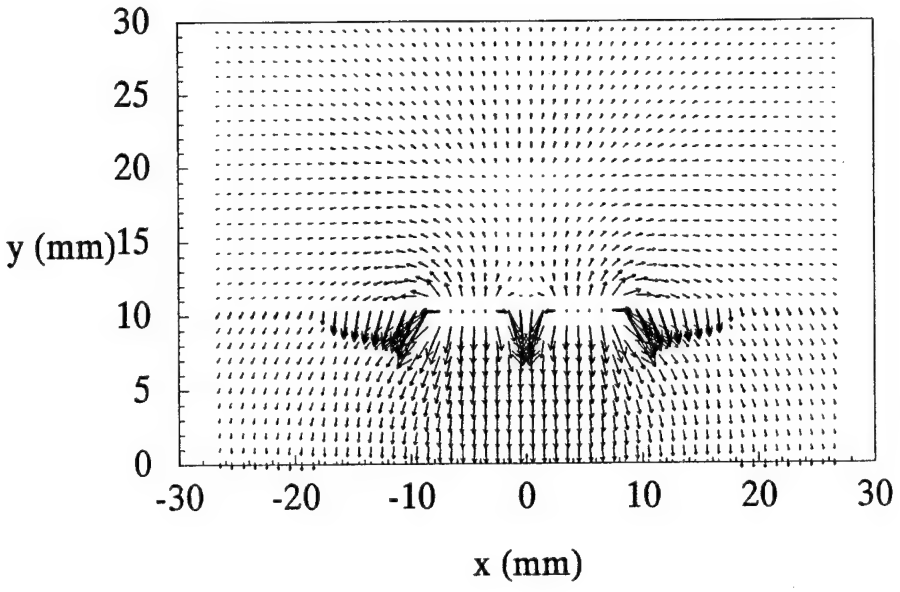

Fig 15 a. Vector map of the electric field, large overlay geometry, even mode, air gap present.

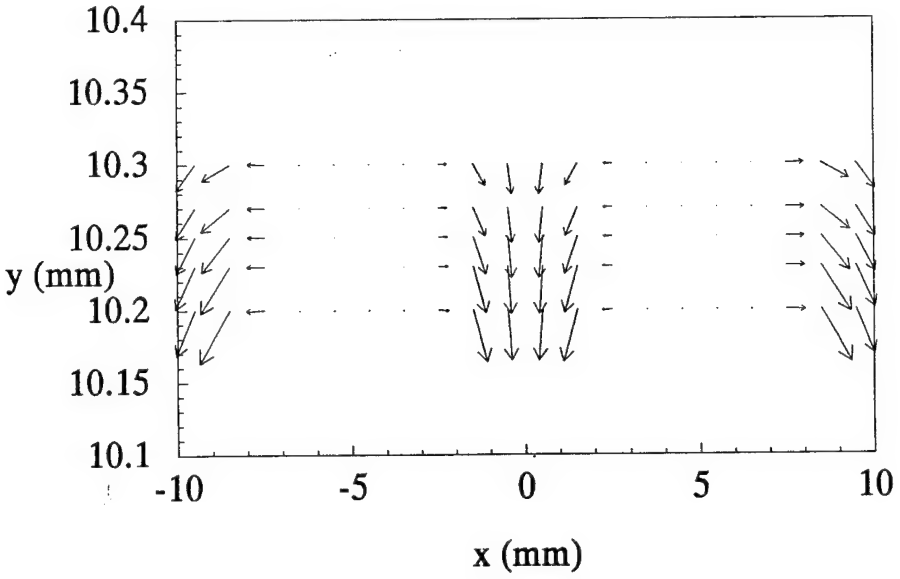

Fig 15 b. Detailed vector map of the electric field between the conductors, large overlay geometry, even mode, air gap present.

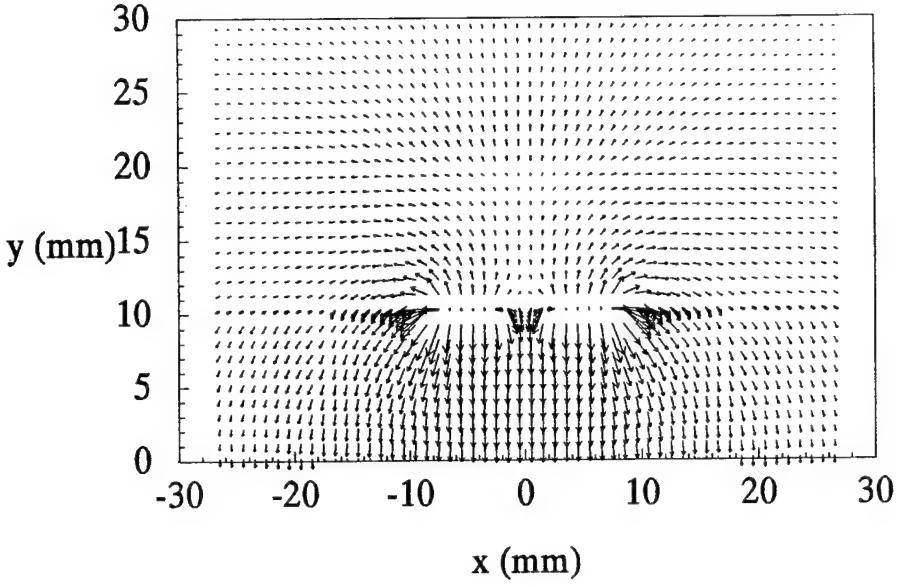

Fig 15 c. Vector map of the electric field, large overlay geometry, even mode, no air gap present.

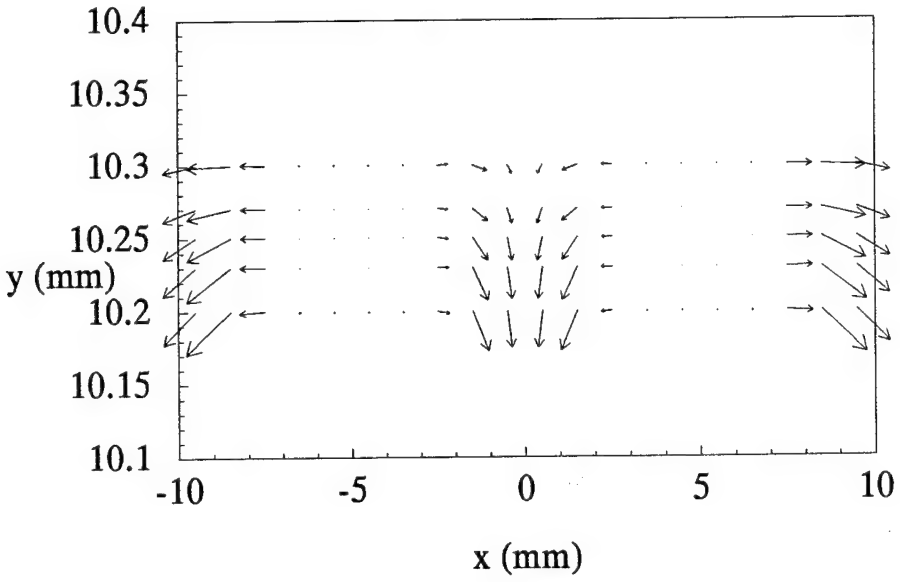

Fig 15 d. Detailed vector map of the electric field between the conductors, large overlay, even mode, no air gap present.

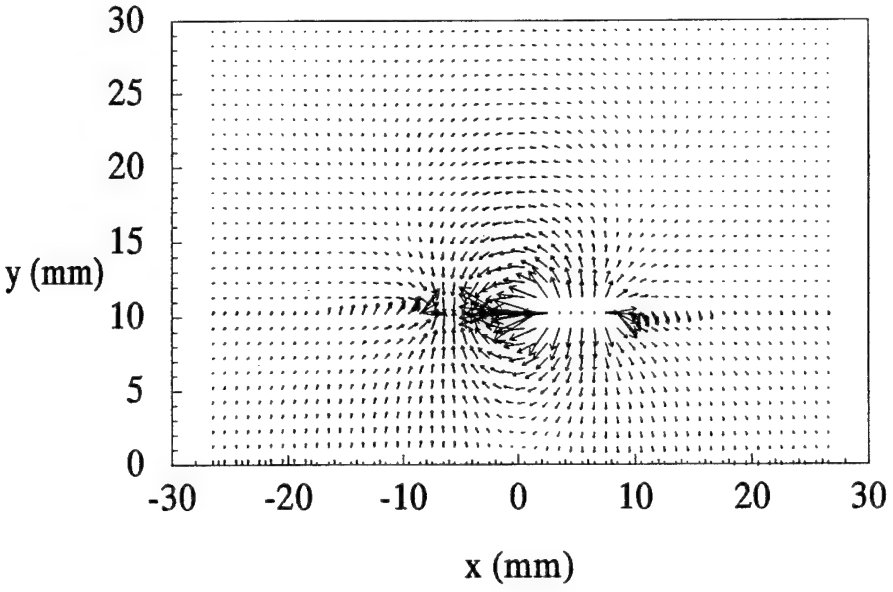

Fig 16 a. Vector map of the electric field, large overlay geometry, odd mode, air gap present.

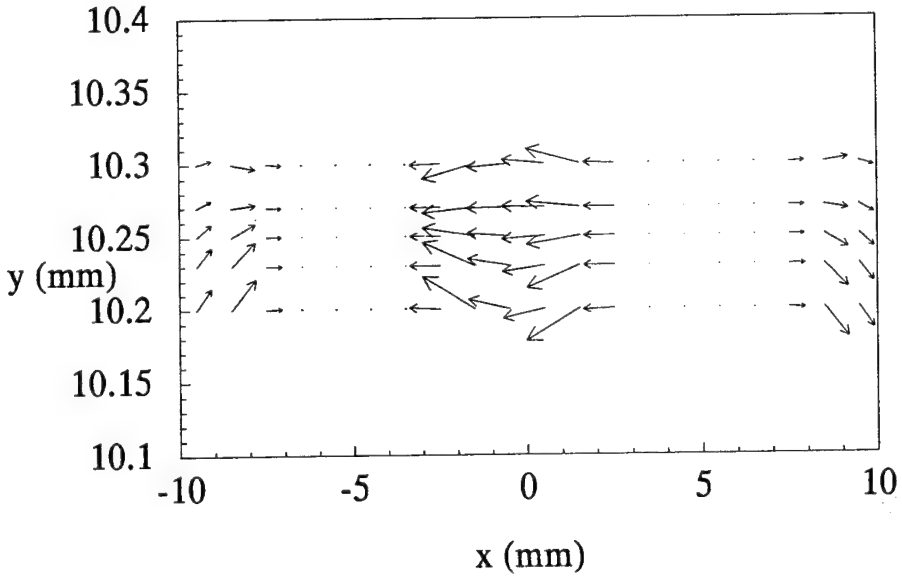

Fig 16 b. Detailed vector map of the electric field between the conductors, large overlay geometry, odd mode, air gap present.

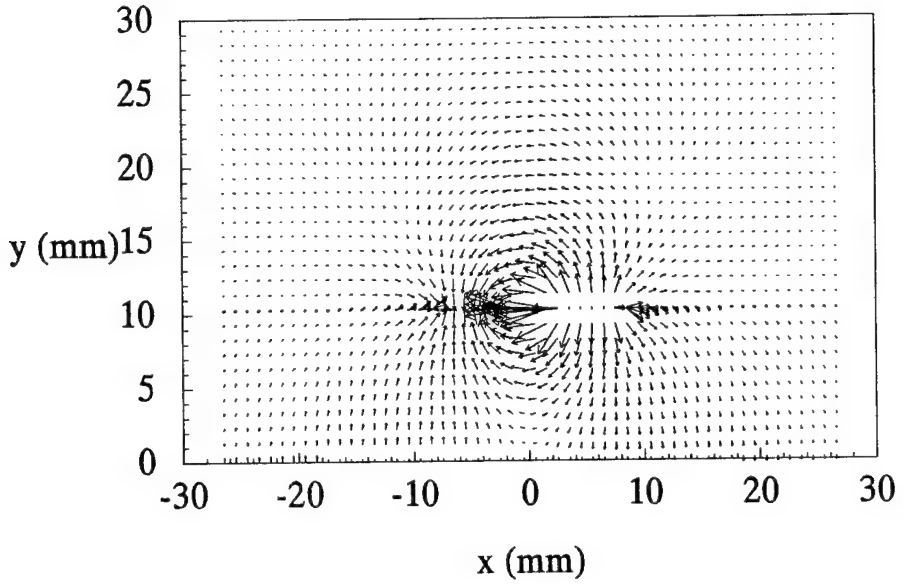

Fig 16 c. Vector map of the electric field, large overlay geometry, odd mode, no air gap present.

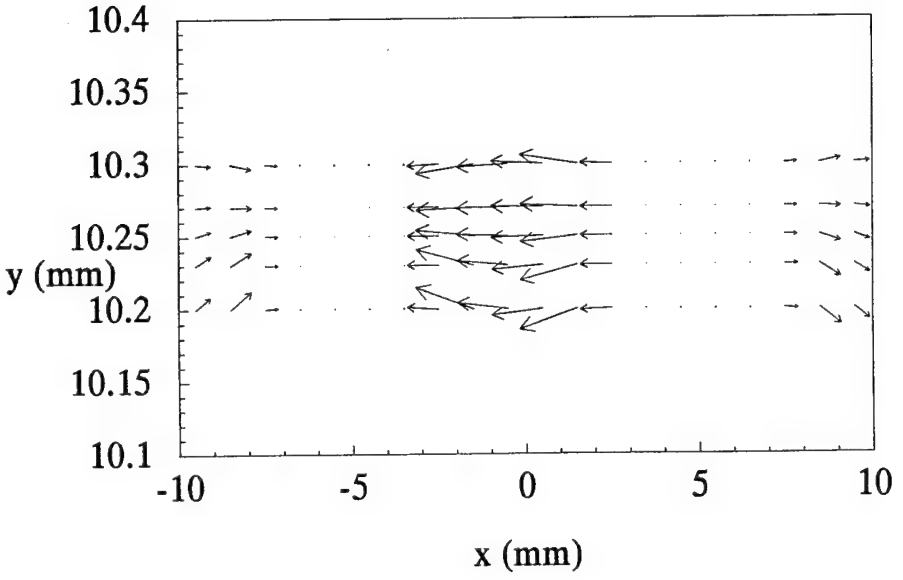

Fig 16 d. Detailed vector map of the electric field between the conductors, large overlay geometry, odd mode, no air gap present.

plane. The height of the substrate was found to be 1.651mm, and the overlay was set to 0.8mm. The substrate extends 5mm from the outer edges of the conductors, while the overlay extends only 2.5mm. The relative permitivity of the substrate was kept at 4.8 while the relative permitivity of the overlay was changed. Like in the previous cases for the large overlay, the presence of the air gap did reduce the coupling, Fig. 17 show the results obtained for the self and mutual capacitances and the coupling coefficient with and without the air gap.. Table III shows the results for the case when the relative permitivity of the overlay is 9.6.

Table IV. Results for the small overlay geometry.

	C_{11}	C_{12}	k_e
No air gap	282.67	35.93	-18.97dB
Air Gap	297.1	30.3	-20.39dB

Figure 18a shows the electric field around the conductors for the even mode. The effect of the air gap is clearly seen and it appears to be stronger for the even mode than for the odd mode shown in Fig. 18b.

F) Coupling on an Asymmetric Transmission Line.

Figure 19 shows two different geometries that were also analyzed. The top one has the conducting strips embedded in the dielectric substrate. The bottom one has the conductors resting above the substrate. Furthermore, the substrate contains different types of dielectric materials. The dimensions of the geometry were the following: The height of the substrate (h) was 0.3mm, the width (w) of the conductors was 0.1mm, the separation between the lines (s) was 0.075mm, and the thickness of the conductors (t) was set to 0.001mm. The substrate was composed of the following materials: polystyrene, silicon, and alumina with dielectric constants of 2.54, 11.9 and 9.6, respectively. The values where taken from Appendix G of [12]. Table V shows a sample of numerical results for both geometries shown in Fig. 19.

Table V. Results from the FD code for the geometries shown in Fig. 19.

Case				Numerical results based on the FD code			
ε_{r1}	ε_{r2}	ε_{r3}	Embedded lines	k_{e12}	k_{e21}	$\varepsilon_{\text{eff even}}$	$\varepsilon_{\text{eff odd}}$
2.54	9.6	9.6	no	-18.96dB	-18.96dB	5.14	3.77
2.54	11.9	11.9	no	-20.15dB	-20.15dB	6.11	4.36
2.54	9.6	11.9	no	-18.87dB	-20.22dB	5.14	3.78
2.54	9.6	9.6	yes	-18.33dB	-18.33dB	5.16	3.86
2.54	11.9	11.9	yes	-19.52dB	-19.52dB	6.14	4.44
2.54	9.6	11.9	yes	-18.25dB	-19.59dB	5.16	3.86

These results show that the presence of air between the conductors reduces the coupling between the lines by approximately 0.5dB. The reduction is not significant compared to the previous cases where an overlay was present. The increase in the dielectric constant of the substrate under the conductor increases the self capacitance on the line. This increase in the self capacitance translates in a reduction of the coupling between the lines.

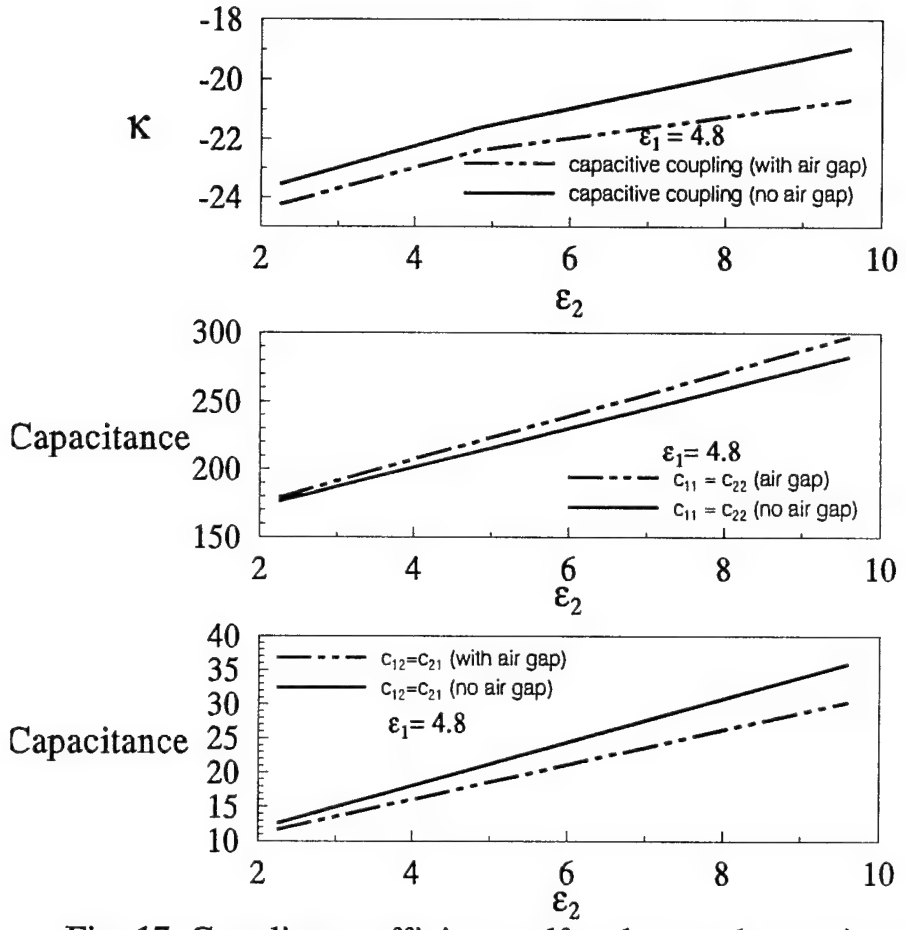

Fig. 17. Coupling coefficient, self and mutual capacitances for different small overlays, with and without air gap.

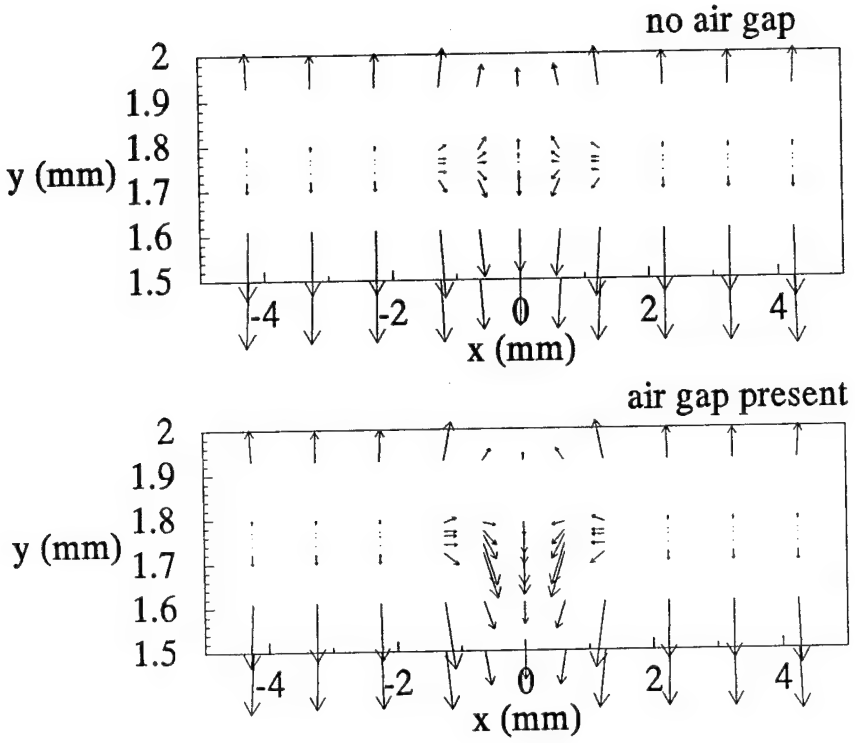

Fig. 18 a. Detailed vector map of the electric field around the conductors for the small overlay geometry with and without the air gap, even mode.

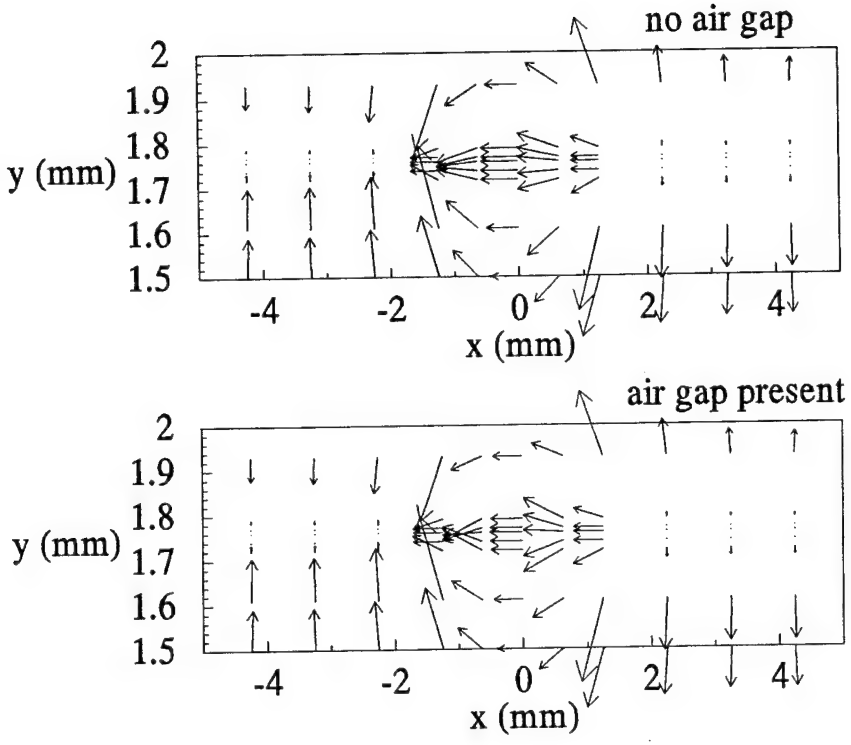

Fig. 18 b. Detailed vector map of the electric field around the conductors for the small overlay geometry with and without the air gap, odd mode.

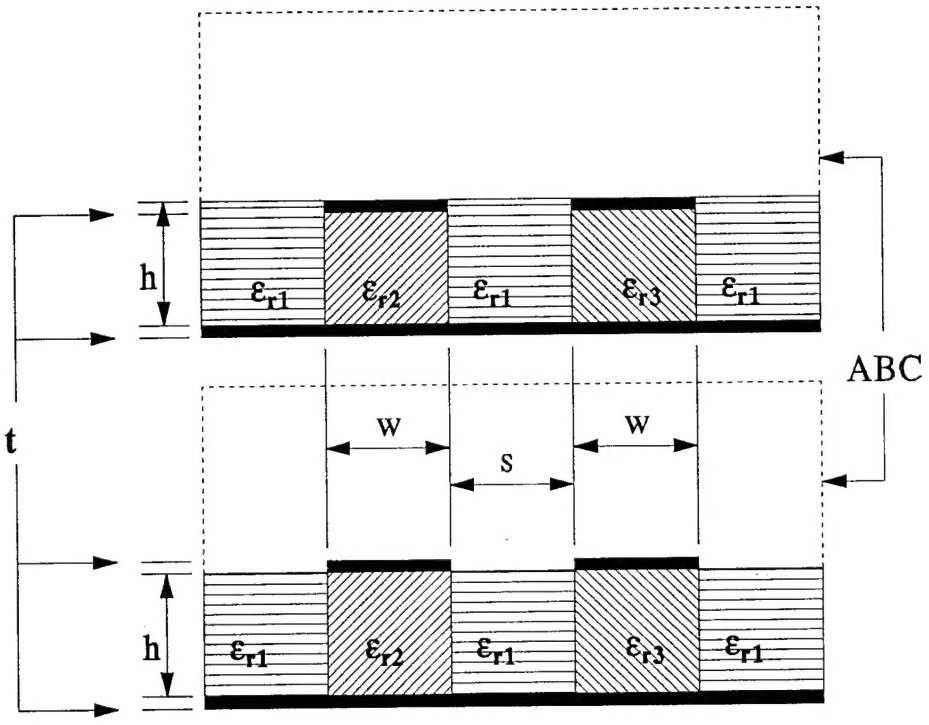

Fig. 19. Two geometries with substrates made out of different dielectrics. One has conductors embedded in the substrate and the other has conductors lying on the substrate.

CHAPTER V
CONCLUSION

The FORTRAN code developed can analyze a large variety of transmission line geometries. The results that have been compared with previously published were very satisfactory. The program has shown that it can deal with complicated geometries containing different dielectric materials and that these geometries may be asymmetric. The effects of the presence of the air gap on the electric field distribution have been shown. These changes lead to a reduction of the capacitive coupling between the lines. However, the coupling may be increased when the relative permitivity of the overlay is large. When building couplers it may be desirable to eliminate the air gap by embedding the lines in the substrate or the overlay. It is also shown that susbtrates with high dielectric constants help reduce the coupling.

VI. REFERENCES

[1] A.Z. Elsherbeni, B. Moumneh, and C. E. Smith," Characteristics of Two-Conductor Microstrip Transmission Lines Embedded in a Ground Plane Using the Finite Difference Technique," *Technical Report 93-3,* Department of Electrical Engineering, University of Mississippi, July, 93.

[2] D. Kahaner, C. Moher, N. Stephen, *Numerical Methods and Software.* Prentice Hall, 1989.

[3] M. N. O. Sadiku, *Numerical Techniques in Electromagnetics*.CRC Press, Boca Raton, Florida, 1992.

[4] A. Khebir, A. B. Kouki, and R. Mittra, " Absorbing Boundary Condition for Quasi-TEM Analysis of Microwave Transmission Lines via the Finite Element Method," *J. Electromagn. Waves and Appl.*, vol. 4, no. 2, 1990.

[5] W. R. Smythe, *Static and Dynamic Electricity*. Hemisphere publishing Company, pp. 63-64, 1989.

[6] A. Z. Elsherbeni, Y. Yuan, and C. E. Smith, "Finite Difference Analysis of a Cylindrical Two Conductor Microstrip Transmission Line With Truncated Dielectrics," *Technical Report 95-1,* Department of Electrical Engineering, University of Mississippi, January,95.

[7] J. J. Dongama, C. B. Maler, J.B. Bunch, and G.W. Stewart, *Linpack User's guide.*

[8] D. Kajfez, *Notes on Microwave Circuits.*, Oxford, Mississippi: Kajfez Consulting, 1986, Vol. 2, Chapter 7

[9] R. K. Hoffmann, *Handbook of Microwave Integrated Circuits*. Norwood: Artech House, pp.232-233 1987.

[10] C. E. Smith, M. D. Tew, and W. Wu, "Use SPICE to Analyze PCB Crosstalk," *EMC Test & Design,* pp.20-27, April 1994.

[11] A. G. Engel, Jr. and P. B. Katehi, "Frequency and Time Domain

Characterization of Microstrip-Ridge Structures," *IEEE Trans. Microw. Theory and Tech.*, Vol. 41, No.8, pp.1251, Aug. 1993.

[12] D. M. Pozar, *Microwave Engineering.*, Addison-Wesley, Reading, Massachusetts. 1990.